

## Figure 1 Theory Meets Figure 2 Experiments in the Study of Gene Expression

Rob Phillips<sup>1,2,\*</sup>, Nathan M. Belliveau<sup>2</sup>, Griffin Chure<sup>2</sup>, Hernan G. Garcia<sup>3</sup>, Manuel Razo-Mejia<sup>2</sup>, Clarissa Scholes<sup>4</sup>

<sup>1</sup> Dept. of Physics, California Institute of Technology, Pasadena, California, U.S.A

<sup>2</sup> Division of Biology and Biological Engineering, California Institute of Technology, Pasadena, California, U.S.A

<sup>3</sup> Department of Molecular & Cell Biology, Department of Physics, Biophysics Graduate Group and Institute for Quantitative Biosciences-QB3, University of California, Berkeley, California, U.S.A

<sup>4</sup> Department of Systems Biology, Harvard Medical School, Boston, Massachusetts, U.S.A

\* E-mail: phillips@pboc.caltech.edu

*“hic rhodus, hic salta” - Aesop’s fables*

### Abstract

It is tempting to believe that we now own the genome. The ability to read and re-write it at will has ushered in a stunning period in the history of science. Nonetheless, there is an Achilles heel exposed by all of the genomic data that has accrued: we still don’t know how to interpret it. Many genes are subject to sophisticated programs of transcriptional regulation, mediated by DNA sequences that harbor binding sites for transcription factors which can up- or down-regulate gene expression depending upon environmental conditions. This gives rise to an input-output function describing how the level of expression depends upon the parameters of the regulated gene – for instance, on the number and type of binding sites in its regulatory sequence. In recent years, the ability to make precision measurements of expression, coupled with the ability to make increasingly sophisticated theoretical predictions, have enabled an explicit dialogue between theory and experiment that holds the promise of covering this genomic Achilles heel. The goal is to reach a predictive understanding of transcriptional regulation that makes it possible to calculate gene expression levels from DNA regulatory sequence. This review focuses on the canonical simple repression motif to ask how well the models that have been used to characterize it actually work. We consider a hierarchy of increasingly sophisticated experiments in which the minimal parameter set learned at one level is applied to make quantitative predictions at the next. We show that these careful quantitative dissections provide a template for a predictive understanding of the many more complex regulatory arrangements found across all domains of life.

### 1. Introduction

The study of transcriptional regulation is one of the centerpieces of modern biology. It was set in motion by the revolutionary work of Jacob and Monod in the postwar era, which culminated in their elucidating the concept of transcriptional regulation in the early 1960s [1, 2, 3], and it has continued apace ever since. Based on their study of the *lac* operon and regulation of the life cycle of bacterial viruses, Jacob and Monod hypothesized that transcription was controlled using a mechanism sometimes known as the repressor-operator model, in which repressive factors bind to promoters at sites called operators to prevent activation of genes. Here, we will refer to this regulatory architecture as the simple-repression motif.

Jacob and Monod suspected that there would be a universal mechanism for transcriptional regulation that followed the strictures of the repressor-operator model; indeed, simple-repression, defined diagrammatically in Figure 1(A), has since been shown to have widespread applicability as seen in Figure 1(B).

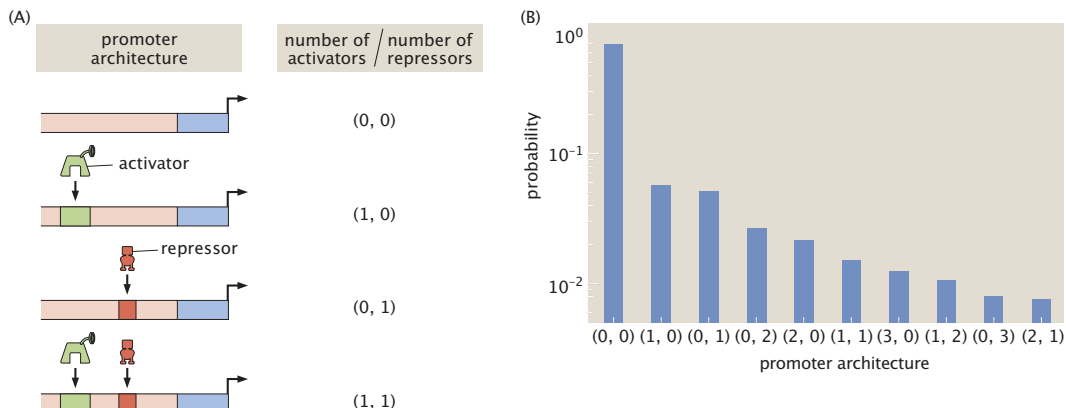


**Figure 1.** The distribution of regulatory architectures in *E. coli*. (A) Several of the simplest regulatory architectures are shown, featuring activator and repressor binding sites. We adopt the notation  $(m, n)$  to characterize these architectures where the first number  $m$  tells us how many activator binding sites there are for our gene of interest and the second number  $n$  tells us how many repressor binding sites are controlling that same gene. Within this notation, a  $(0, 0)$  architecture is unregulated, a  $(1, 0)$  architecture is a simple activation motif and a  $(0, 1)$  architecture is a simple repression motif and is the central focus of the present article. (B) Relative probability of different classes of regulatory architecture for those genes that have been annotated in *E. coli* [7, 8]. For transcription factors that can act both as activators and repressors, we consider their specific mode of action in the context of each regulatory architecture. For example, if a transcription factor binds to a single site near a promoter and acts as an activator, we consider it to fall within the  $(1, 0)$  nomenclature even if this same protein can act as a repressor on other regulatory units.

However, transcriptional reality is – as is usually the case in biology – far more complicated [4], and, as Figure 1 reveals, many genes are in fact subject to both negative and positive regulation. Ironically, the genetic circuit used by Monod to formulate the repressor-operator model – the *lac* operon shown in Figure 2 – is itself subject to positive regulation, which shows the repressor-operator model to be incomplete [5, 6].

The *lac* operon is one of the canonical case studies learned by high-school and college students alike when they are first introduced to the logic of gene regulation in modern molecular and cellular biology [9, 10]. Figure 2 shows in cartoon form how the gene that encodes the enzyme for digesting lactose is activated only when lactose is present and glucose is absent. This textbook case of transcriptional regulation has been studied to death, but how well do we really understand it? The sketch in Figure 2 is a broad-brush view of transcriptional control at the *lac* operon, but it gives us no sense of how the level of gene expression is affected by, for example, changing the copy numbers of the LacI and CRP transcription factors, changing the positioning of the operator, or titrating the relative concentrations of glucose and lactose. We argue that achieving real understanding of this system requires that we are capable of making precise and quantitative predictions about its regulatory response as a function of all these parameters, and then that we are able to confirm these predictions experimentally.

How could we achieve this mastery? First, we would need theoretical models able to provide quantitative predictions that can be tested with careful experiments. Importantly, both the predictions and the experiments themselves would need to access the same underlying knobs to control the level of gene expression. Second, we would need to start with the simplest of regulatory architectures. If we are unable to understand the most basic regulatory kernel, we have no hope of doing so for more complex regulatory circuits. Third, to dissect more subtle features of a regulatory circuit – for instance, to understand how expression noise depends on changing parameters – we must be able to use quantitative information gleaned from one type of experiment to formulate further predictions that are tested in subsequent experiments of a different type. Therefore, we would need to conduct all these experiments in the same system and under standardized conditions.

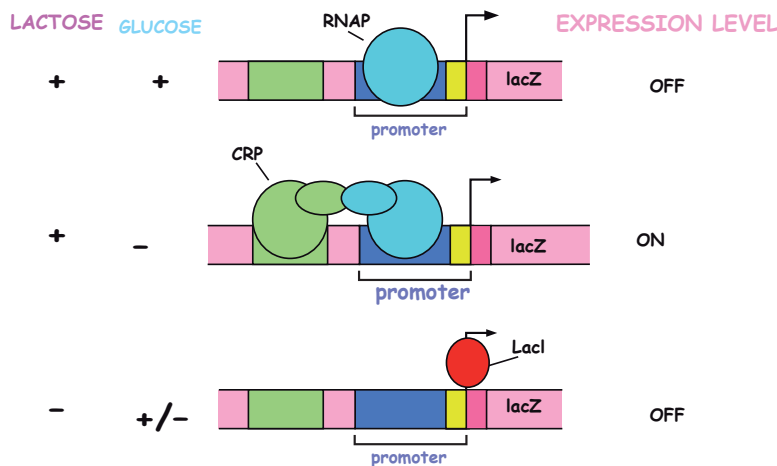


**Figure 2.** The high school *lac* operon. The classic story of how bacteria utilize lactose rather than glucose as a carbon source is the canonical example used to teach the concept of genetic regulation. The figure shows that only when lactose is present and glucose is absent will the gene for the enzyme used to digest lactose be turned on. The activator is shown in green, the repressor is shown in red, and RNA polymerase is depicted in blue.

This review summarizes such an approach, which we have taken in our own laboratory over the past decade. We discuss how, working with a set of specifically-designed synthetic constructs and challenging theoretical models with experiments, we have been able to tackle increasingly subtle behaviors of the simple repression architecture in *E. coli*. The strategy we have taken results in a pyramidal structure, as shown in Figure 3, in which parameters inferred at one level are used to make quantitative predictions about gene expression behavior in successive, more sophisticated experiments.

At the foundation of the simple repression pyramid are experiments to determine how gene expression responds to changes in operator strength and repressor copy number. With this information in hand, we can then consider the entire distribution of expression levels among a population of cells, as opposed to simply the average expression. At the next level in the hierarchy, we address a number of subtle and beautiful effects that arise when there is more than one copy of our gene of interest or competing binding sites for the repressor elsewhere on the genome (or on plasmids). This repressor titration effect provides a very stringent test of our understanding of the simple repression motif. Of course, much of gene expression is dictated by the presence of environmental signals and the next level in the simple repression pyramid is to ensure that these same kind of predictive models can describe induction of transcription. Further, changes in the environment such as media quality or growth temperature certainly have an effect on the bacterial doubling rate. The next challenge is then to retain predictive power by describing how these different conditions affect the magnitude of parameters that are the basis of these models, such as repressor copy number and binding energy. Finally, evolution of transcription acts both at the level of transcription factor binding sites and the transcription factors that bind to them. Ultimately, the simple repression pyramid will be topped off by learning the rules that relate transcriptional regulation to fitness [11, 12, 13, 14]. At every level in the pyramid, we demand that the parameters be self-consistent. That is, regardless of how our experiments are done or which new question we ask, the same minimal parameter set is used without recourse to new fits for each new experiment.

Note that this paper is not a review of a field; rather it is a review of a concept, in which one minimal parameter set is asked to describe all measurements on a particular realization of the simple-repression motif. This objective is not served by an approach in which different measurements are taken from disparate sources on different strains under different conditions. We focus instead on measurements made using the same strains under the same growth conditions throughout, and this renders the discussion

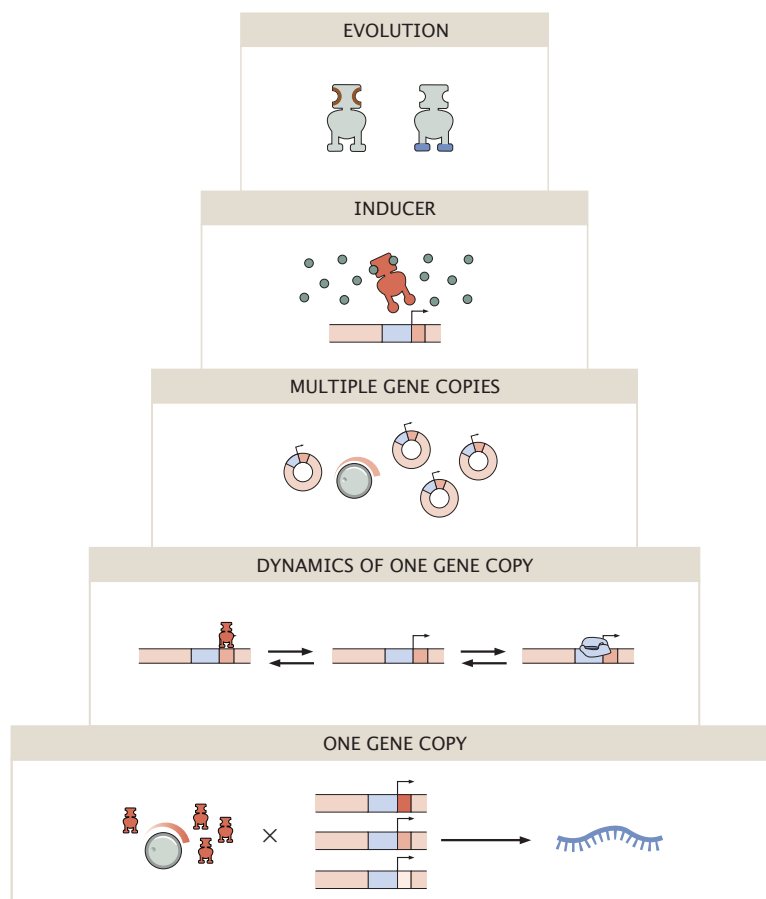


**Figure 3.** The simple repression pyramid. A progression of different experiments makes it possible to assess increasingly subtle regulatory effects for the simple repression motif. Parameters inferred from lower levels in the pyramid are used in the analysis of the experiments at the next level. The repressor (and its binding site) is shown in red, RNAP polymerase (and its binding site) is shown in blue, and inducer in green.

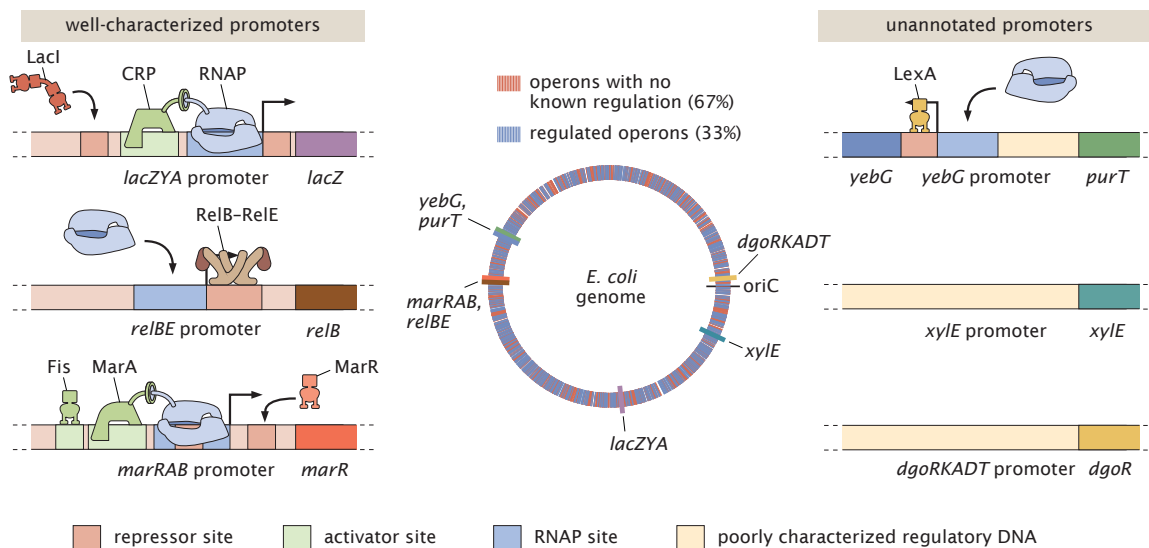


**Figure 4.** Regulatory ignorance in *E. coli*. The central figure which schematizes the *E. coli* genome shows the fraction of the operons for which we know nothing about how they are regulated. The left panels show examples of the knowledge of regulatory architectures required to unleash the kind of theory-experiment dialogue described here. The right side panel shows the more common situation which is complete regulatory ignorance.

highly self-referential. But everything we have done was enabled by beautiful work that has come before and inspired by wonderful experiments since; we point the reader towards as much of this literature as possible.

The goal of this review is to address whether, for simple repression, we have reached a self-consistent theoretical picture that stands up to careful experimental scrutiny. After an overview of regulatory architectures in *E. coli*, and the simple repression motif in particular, we describe our systematic effort to make the strains, tune the relevant knobs, and make the high precision measurements that enable us to test theoretical predictions about how the simple repression architecture behaves. In the following sections we then address the key critiques of the theoretical framework, before stepping back to discuss what our results entail for future efforts in understanding gene regulation. We argue that we have achieved significant success using this hierarchical approach and that it provides hope for understanding other, more complex, gene regulatory circuits. Indeed, the great work done by others in *lac* [15, 16, 17], MarA [18, 19], GalR [20, 21, 22], Lambda [23, 24, 25, 26], and AraC [27] lends itself to providing the fundamental stepping stones for building other transcriptional pyramids.

## 2. The Regulatory Landscape in *E. coli* and the Ubiquitous Simple Repression Architecture

Despite the dominance of *E. coli* as a model system for studying gene regulation, we remarkably have little or no idea how most of its genes are controlled. As Figure 4 demonstrates, for the majority of genes we don't know the identity of the transcription factors that turn them on/off, where the binding motifs for those transcription factors are, or what the regulatory logic is (at the most basic level, whether they are controlled by repressors, activators or a combination of both). Figure 1 provides an incomplete, but state-of-the-art picture of our current knowledge of the regulatory landscape by showing the distribution of different architecture types in *E. coli*. Shortly after the elucidation of the repressor-operator model (the (0,1) motif) that introduced the simple repression architecture we focus on here, the idea of activation as a regulatory mechanism also took root. But as we see in Figure 1(B), at the time of this writing, most genes in *E. coli* are annotated as unregulated. This sounds counterintuitive, but for many genes it

likely reflects ignorance of the binding motifs and regulators as opposed to actual lack of any regulation. Simple repression (along with simple activation) comes in as the next most prevalent architecture, and we now turn our attention there.

Simple repression is a common regulatory motif in *E. coli* [7], but we know little of the general principles by which it is used. To tackle this, we used annotated regulatory information from RegulonDB [8] to survey 156 promoters with a simple repression architecture, controlled by 50 different transcription factors. We first wanted to know how the concentrations of these regulators change under different growth conditions, and how this relates to their probability of binding to the promoters in question.

To characterize each promoter, we used published data that quantified protein abundance across the bacterial proteome under various growth conditions using either ribosomal profiling or mass spectrometry [28, 29]. Figure 5(A) shows the distribution of repressor and activator copy numbers genome wide, while Figure 5(B) shows the copy numbers for just those repressors that target the (0,1) architectures in which we are interested. The transcription factors vary in copy number from 0 to about 10,000 per cell. Of the repressors, just over half of them bind 10 or fewer binding sites, while some targeted over 100 binding sites across the genome (Figure 5(E)). Given the wide range in repressor copy number, we wondered whether it related to the number of target binding sites that exist for each of these repressors in the genome. Indeed, when we calculated the ratio between protein copy number and number of target binding sites for each transcription factor (as indicated by the dashed lines in Figure 5(B)) we found a median ratio of about 15 transcription factor copies per binding site. The majority of the transcription factors (about 80%) have no more than 100 copies per binding site. Given that the number of transcription factors per binding site is on the order of 10 - 100, we can infer that their typical effective binding constants (defined in detail below) are in the 10 - 100 nM range, since 1 copy of a protein per bacterial cell corresponds to a concentration of roughly 1 nM.

We next asked how these simple repression promoters are regulated by the transcriptional repressors that control them. It might be the case that the promoters respond to changes in repressor copy number; alternatively, the copy number may remain constant but a repressor be induced by an external signal to switch to an active state. Using mass spectrometry measurements of protein copy number across 22 growth conditions (varying carbon source, minimal versus rich media, temperature, pH, growth phase, osmotic shock, and growth in chemostats), Schmidt *et al.*, 2016 [29] had found that most repressor copy numbers do not vary dramatically as a function of growth condition (Figure 5(C)). Figure 5(D) gives a quantitative picture of the variability in transcription factor copy number for the repressors that target simple repression architectures. Most repressors exhibit a low coefficient of variation (standard deviation/mean copy number) in their abundance across these growth conditions (median coefficient of variation of 0.33, compared with an 0.51 across the entire proteome). In Figure 6 we replot these data to show how the total proteome changes as a function of growth rate, as compared to how the total number of transcription factors or copies of LacI do. This plot provides a more nuanced picture of the challenges theoretical models must face in treating expression levels over all growth conditions as will be discussed in the final section of the paper.

While it is possible that the growth conditions considered were not appropriate to elicit major changes in the copy number of each repressor, an alternative explanation of the low variability in repressor copy number is that these transcription factors, instead of relying on the modulation of their copy number, depend on ligand binding and allosteric transitions to alter their potency in regulating transcription. Ligand binding followed by conformational changes between inactive and active conformations provide allosteric control of the repressors by altering their DNA binding strength, allowing for immediate changes in gene expression without relying on the much slower process of changing the transcription factor copy number through protein synthesis or degradation. As shown in Figure 5(F), we indeed find that the majority of these repressors (65%) are either known to bind DNA in response to binding to a ligand, or for those less well-characterized, predicted to have a ligand binding domain. In addition, several of the other repressors that were identified are part of two-component systems that bind DNA in a

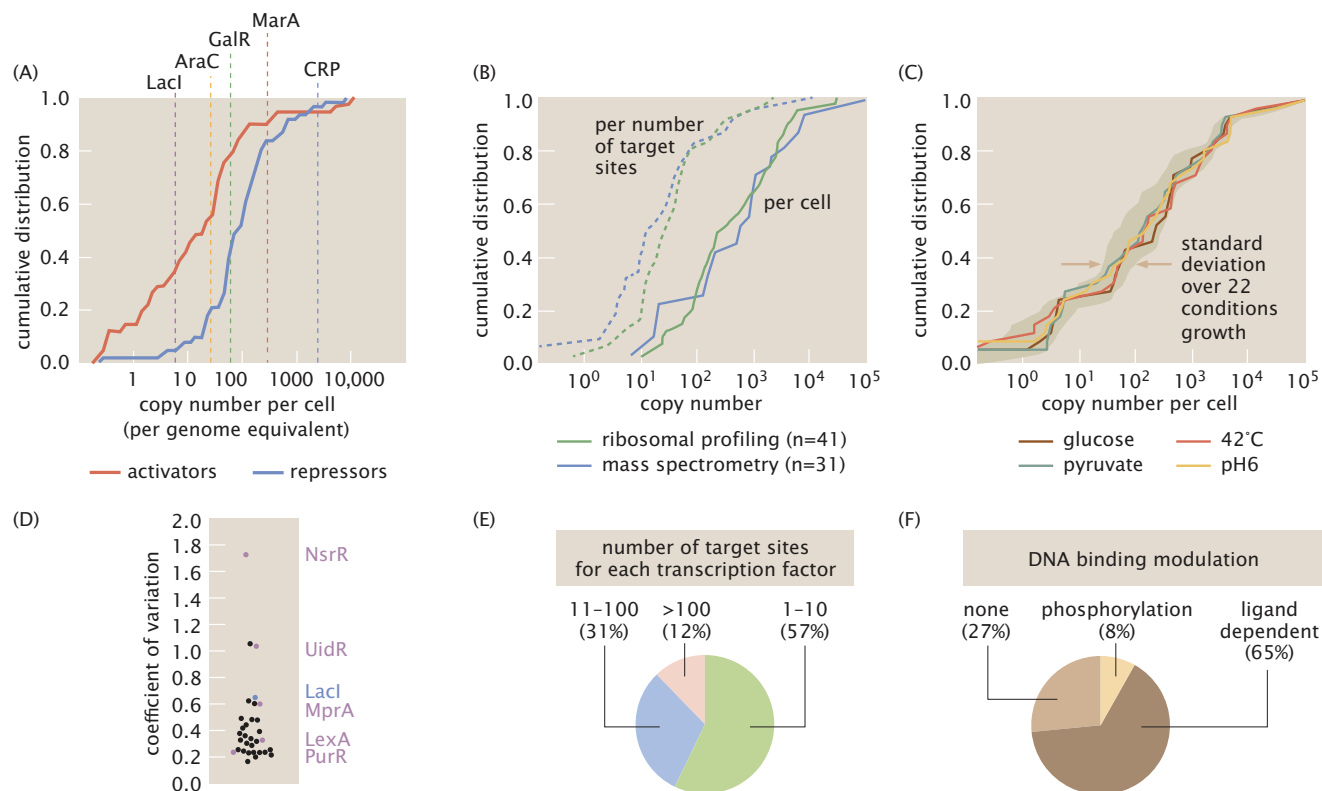


**Figure 5.** Summary of transcription factors that target the (0,1) simple repression architecture. (A) Transcription factor copy numbers in *E. coli* [28]. The cumulative distribution of transcription factor copy numbers indicates that activator copy numbers are generally lower than repressor copy numbers. Roughly half of the activators have copy number less than 10 while roughly half of all repressors have copy number less than 100. Several representative examples of well known transcription factors are shown for reference. (B) Cumulative distributions are shown for transcription factors that target the (0,1) simple repression architecture. Data is shown from measurements using ribosomal profiling (41 of the 50 identified repressors were measured in MOPS minimal media with 0.2% glucose; [28]) and mass spectrometry (31 of the 50 identified repressors were measured in M9 minimal media with 0.5% glucose; [29]). (C) The variability in cumulative distribution is shown for the 31 transcription factors regulating the (0,1) architecture measured across 22 different growth conditions, using mass spectrometry. The shaded region represents the 95th percentile region in cumulative distributions across growth conditions, with the distributions for four growth conditions shown explicitly. (D) Coefficient of variation for copy numbers of transcription factors regulating the (0,1) architecture across the 22 different growth conditions, measured by mass spectrometry. Several examples are identified along with LacI and the complete list is summarized in Table 1. (E) Number of target binding sites for each of the transcription factors that target a (0,1) architecture (using annotated information from RegulonDB [8]). (F) Mechanisms of target binding modulation for transcription factors that target a (0,1) architecture. Ligand-dependent transcription factors contain a known or predicted protein domain for binding by a ligand (using information from EcoCyc [30]).

phosphorylation-dependent manner.

### 3. Simple Repression as the Hydrogen Atom of Gene Regulation: Hic Rhodus, Hic Salta

In physics, when we establish some model system that shows our complete command of an area, it is often christened “the hydrogen atom” of that subject. This badge of honor refers to the far-reaching power of the hydrogen atom in the context of the modern quantum theory of matter. The theory not only informs the classic analysis of spectral lines in hydrogen, but also many more nuanced behaviors ranging from the Stark and Zeeman effects to some of the most subtle effects seen in quantum electrodynamics [31]. Using

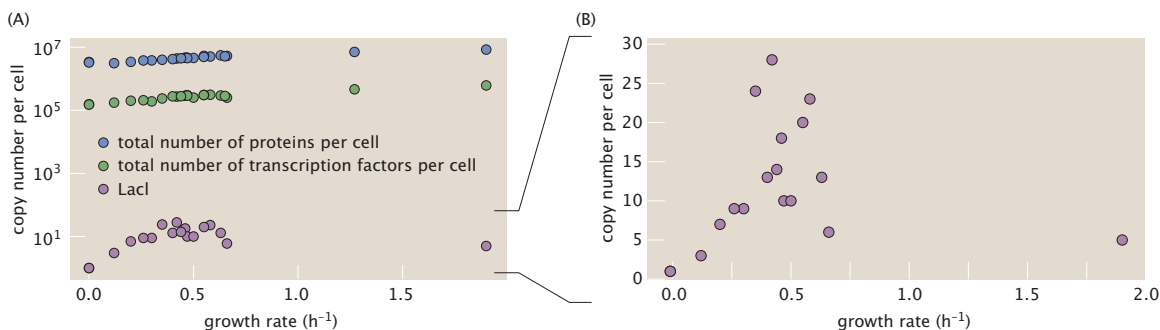


**Figure 6.** Protein census in *E. coli* as a function of growth rate. The figure shows the cellular copy number for all proteins, only transcription factors, and for LacI. The low copy number observed for LacI exemplifies the low protein counts that are commonly observed for such regulatory proteins. Each growth rate represents a different growth condition that was considered in the work of Schmidt *et al.* [29].

the tools of quantum mechanics, the hydrogen atom is simple enough to explore – both mathematically and experimentally – many of the most important ideas in modern physics. It can also teach us what a solution to the problem looks like, in a way that is instructive when going on to tackle more complicated problems such as the behavior of heavier atoms.

We argue that this analogy is helpful in thinking about the simple repression motif as a foundation for launching into the study of more complicated regulatory architectures. One of Aesop’s fables recounts the exploits of a braggart who after a trip to the island of Rhodes claimed to have made a long jump that could not be equaled by others. A witness to the braggart’s commentary replied “*hic rhodus, hic salta*” meaning, “Here is your Rhodes, jump now”. The simple repression motif is our Rhodes. Here, we take the leap to see the extent to which we can construct predictive theoretical models for how this regulatory circuit behaves.

The simple repression motif that forms the basis of our work was originally constructed by Oehler and colleagues [32, 33]. In a set of now classic experiments, they pared down the complex *lac* operon and rewired it as a powerful model system, stripped of all but its most essential features. As shown in Figure 7, Oehler *et al.* reduced the number of repressor binding sites (operators) from three to one, creating precisely the repressor-operator model originally envisaged by Jacob and Monod. This remaining binding site was placed so as to compete directly with RNA polymerase for promoter binding. Oehler *et al.* furthermore recognized the key control parameters for the simple repression motif – the repressor copy number and the operator binding strength – and figured out how to manipulate them over different values in parameter space as shown in Figure 8. Using the DNA sequence of the binding site as a way to manipulate its affinity, they could then tune the strength of repression, providing a well-conceived model system for testing the theoretical predictions of various modeling frameworks aimed at describing transcriptional regulation. We now consider the kinds of theoretical predictions needed to carry out the experiment-theory dialogue advocated here.

#### 4. Mathematicizing Transcriptional Regulation

While some may say that Figure 2 makes predictions as to when gene expression will be turned “on” or “off”, we protest this loose use of the term “prediction” which in our minds has a very special meaning. To earn the title of “the hydrogen atom of X”, one must understand the system not only qualitatively, but with quantitative precision as well. In this article, “prediction” is used with care to emphasize the quantitative concreteness of our thinking. Our aim in the coming sections is to examine the myriad of different physical/mathematical approaches that have been set forth to think about gene regulation



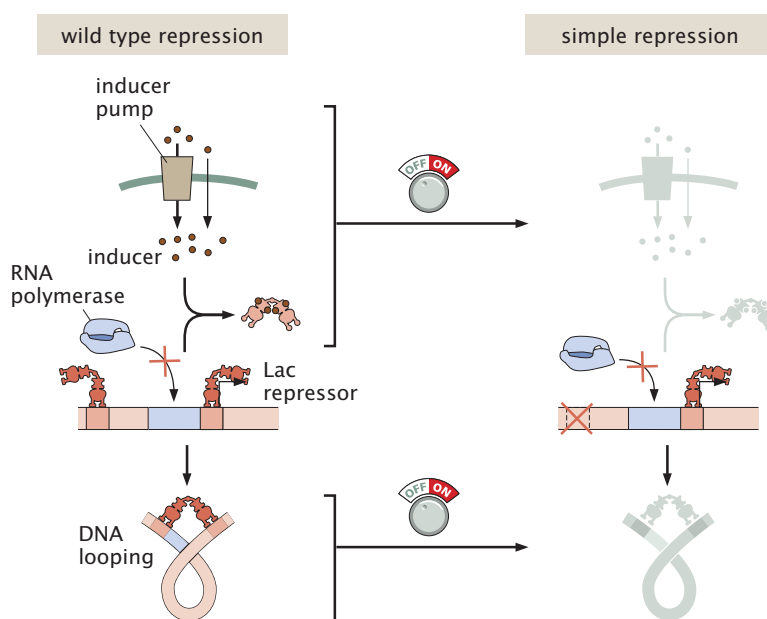


**Figure 7.** Deconstructing the *lac* operon to make the simple repression hydrogen atom. Key features of the wild-type *lac* operon such as DNA looping are removed from the architecture to turn it into a model (0,1) architecture.

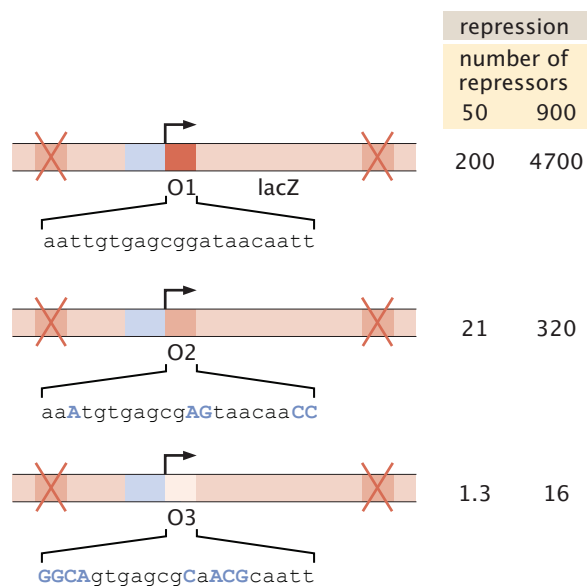


**Figure 8.** Classic experiments reveal key regulatory knobs of the simple repression motif. Oehler *et al.* deleted the auxiliary binding sites in the *lac* operon rendering it into a simple repression architecture [32, 33]. Different operators were used as the repressor binding site and several different repressor counts were tuned resulting in different values of the repression, defined as the ratio of gene expression with no repressors present to the level of expression with repressors present. Changes to operator sequence with respect to the O1 operator are highlighted in blue.

in a predictive fashion. Figure 9 shows the different classes of models that will be entertained in the remainder of the article as a result of their prevalence in the literature and their impact on the field itself. Figure 9(A) provides a schematic of how thermodynamic models are used to compute promoter occupancy, an approach that will be described in greater detail below. Figure 9(B) focuses instead on mRNA dynamics using differential equations to account for the mean number of mRNA as a function of time given the microscopic processes that lead to both an increase and decrease in the number of mRNAs. An even more ambitious strategy is presented in Figure 9(C) which focuses on the dynamics of the full distribution  $p(m, t)$ , which is defined as the probability of finding  $m$  mRNAs at time  $t$ . To be concrete, our strategy is to focus on the use of each of these different methods in the specific case of simple repression with special focus on what the different classes of models say and how experiments have been used to test those predictions.

#### 4.1. The Occupancy Hypothesis and Thermodynamic Models

The thermodynamic models presented schematically in Figure 9(A) implicitly assume one of the most important and ubiquitous assumptions in all of regulatory biology, namely, the *occupancy hypothesis*. This hypothesis, which will be described, criticized and contrasted with experiments in detail in Appendix 11, informs approaches ranging from the bioinformatic search for transcription factors to the use of ChIP-Seq experiments to the kinds of thermodynamic models that are our focus here. Stated simply, the central assumption is that the rate of mRNA production is proportional to the probability of RNA polymerase occupancy at the promoter,

$$\frac{dm}{dt} = r p_{bound}, \quad (1)$$

where we introduce the notation  $p_{bound}$  for the probability that RNA polymerase is bound to the promoter of interest. More generally, if we have  $N$  transcriptionally active states (e.g. polymerase by itself, polymerase and activator together), then we write

$$\frac{dm}{dt} = \sum_{i=1}^N r_i p_i. \quad (2)$$

The idea behind this equation is that the net average rate of transcription is given by the fraction of time the promoter spends in each transcriptionally active state,  $p_i$ , multiplied by the rate of transcription corresponding to that state,  $r_i$ .

But before we can use this result, we need to know the physical nature of the individual states and how to compute their probabilities. We adopt notation in which the probability of the  $i^{th}$  transcriptionally active state can be thought of as

$$p_i = p_i([TF_1], [TF_2], \dots) \quad (3)$$

where the notation indicates that this probability is a function that reflects the occupancy of the regulatory DNA by the various transcription factors (i.e. regulatory proteins) that interact with the regulatory apparatus of the gene of interest. Hence, each transcriptionally-active state denoted by the label “ $i$ ”, corresponds to a different state of the promoter characterized by a different constellation of bound transcription factors. These ideas were first put into play in the gene regulatory setting by Ackers and coworkers and have since been explored more deeply by number of groups [35, 36, 37, 38, 39, 34, 40, 41, 42, 17]. For the case of the simple repression motif, the thermodynamic model is illustrated in Figure 10.

As in Figure 9(A), the idea is to identify the relevant microscopic states of the promoter and to assign to each such state its corresponding statistical weight. The details of how to use statistical mechanics to compute this probability has been described elsewhere [34, 43] so here we resort to simply quoting the central result of the thermodynamic models for the simple repression motif, namely, the probability of

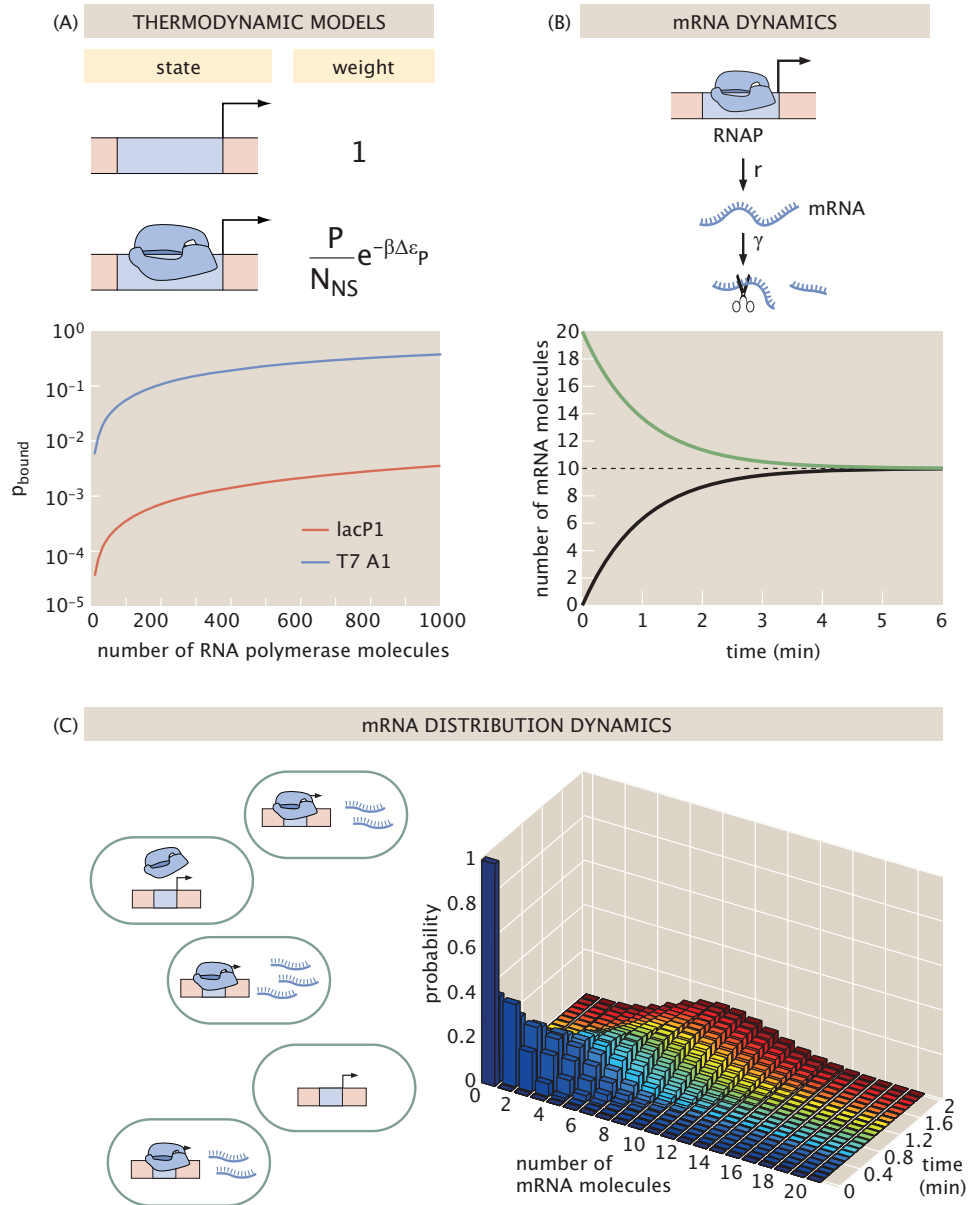


**Figure 9.** Summary of approaches to computing the level of expression from the simple unregulated promoter. These same approaches can be used for computing the response of more complex regulatory architectures such as the simple repression motif that is the central preoccupation of this article. (A) Thermodynamic models compute the probability of promoter occupancy using the Boltzmann distribution. The graph shows the probability of promoter occupancy for a weak (*lacP1*) and a strong (T7 A1) promoter sequence as a function of the number of polymerases. (B) Dynamics of mean expression using kinetic models. The graph shows the number of mRNA molecules as a function of time with the steady-state number shown as a dashed black line. The mRNA dynamics corresponding to two different initial conditions are shown. (C) Dynamics of mRNA distribution using the chemical master equation approach. The bar graph shows how the *distribution* of mRNA copy numbers changes over time, ultimately settling on a steady-state Poisson distribution. (A, adapted from [34]; B and C,  $r = 10$  mRNA/min and  $\gamma = 1 \text{ min}^{-1}$ )

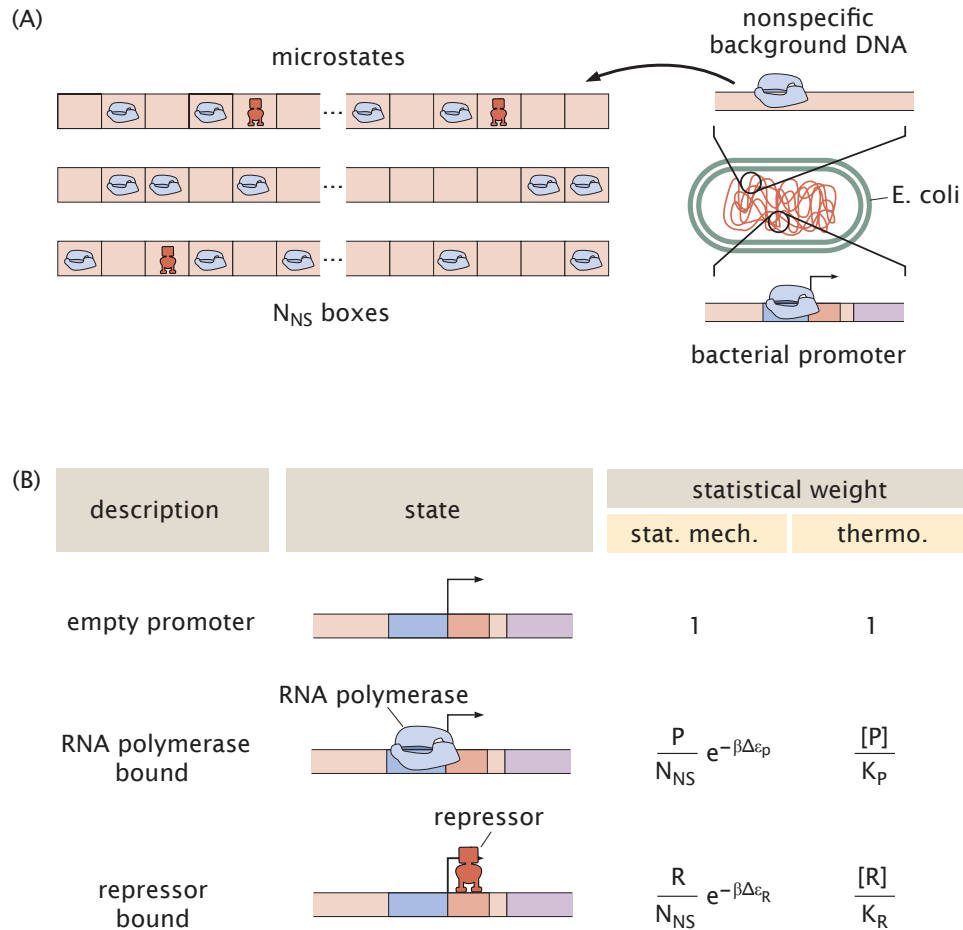


**Figure 10.** States and weights for the simple repression motif. (A) Our regulatory system is assumed to consist of  $P$  RNA polymerase (blue) and  $R$  repressors (red) per cell that either bind nonspecifically to the genomic background DNA (our reference energy state) or compete for binding to our promoter of interest. The genomic background is discretized by assuming a number of potential binding sites,  $N_{NS}$ , that is given by the length of the genome ( $N_{NS} = 4.6 \times 10^6$  for *E. coli*). (B) The different regulatory states of our simple repression promoter. The statistical weight associated with each state is shown using the statistical mechanical and thermodynamic formulations. The binding energies of the  $R$  repressors and  $P$  RNA polymerase to their binding sites on the promoter are given by  $\Delta\varepsilon_R$  and  $\Delta\varepsilon_P$ , respectively. These energies are given relative to the energy of nonspecific binding to the genomic background. In the thermodynamic formulation,  $[P]$  and  $[R]$  are the cellular concentrations of the RNA polymerase and repressor, respectively. Their dissociation constants are given by  $K_P$  and  $K_R$ .  $N_{NS}$  represents the number of nonspecific binding sites for both RNA polymerase and repressor.

finding RNA polymerase bound to the promoter given by

$$p_{bound} = \frac{\frac{P}{N_{NS}} e^{-\beta \Delta \varepsilon_P}}{1 + \frac{P}{N_{NS}} e^{-\beta \Delta \varepsilon_P} + \frac{R}{N_{NS}} e^{-\beta \Delta \varepsilon_R}}, \quad (4)$$

where  $R$  is the number of repressors,  $N_{NS}$  is the size of the genome (i.e. number of nonspecific sites) and  $\Delta \varepsilon_R$  is the binding energy of repressor to its operator. Similarly,  $P$  is the number of RNA polymerase molecules and  $\Delta \varepsilon_P$  is its binding energy to the promoter.

In the language of these models, we can now relate the experimentally measurable repression, which is obtained by quantifying the rate of mRNA production, or the steady state levels of mRNA or protein, in the presence and absence of repressor, to the theoretically calculable quantity  $p_{bound}$  such that

$$\text{repression} = \frac{dm/dt(R=0)}{dm/dt(R \neq 0)} = \frac{rp_{bound}(R=0)}{rp_{bound}(R \neq 0)} = \frac{p_{bound}(R=0)}{p_{bound}(R \neq 0)}, \quad (5)$$

Alternatively, we can write the fold-change as

$$\text{fold-change} = \frac{p_{bound}(R \neq 0)}{p_{bound}(R=0)}, \quad (6)$$

where we have made use of the occupancy hypothesis introduced in Equation 1. We now use the expression for  $p_{bound}$  from Equation 4 and obtain

$$\text{fold-change} = \frac{1 + \frac{P}{N_{NS}} e^{-\beta \Delta \varepsilon_P}}{1 + \frac{P}{N_{NS}} e^{-\beta \Delta \varepsilon_P} + \frac{R}{N_{NS}} e^{-\beta \Delta \varepsilon_P}}. \quad (7)$$

Finally, we assume that binding of RNA polymerase to the promoter is weak such that  $P/N_{NS} e^{-\beta \Delta \varepsilon_P} \ll 1$ . In the context of this weak promoter approximation, which is discussed in detail in [34, 44], the fold-change reduces to

$$\text{fold-change} = \frac{1}{1 + \frac{R}{N_{NS}} e^{-\beta \Delta \varepsilon_R}}. \quad (8)$$

The conceptual backdrop to this result is shown in Figure 10. As we will describe in great detail later in this article and in Appendix 12, there is much confusion about the mapping between statistical mechanics language, which we believe is more microscopically transparent, and thermodynamic language using dissociation constants. In that language, our result for fold-change can be written as

$$\text{fold-change} = \frac{1}{1 + \frac{[R]}{K_R}}, \quad (9)$$

where  $[R]$  is the concentration of repressor and  $K_R$  its dissociation constant to operator DNA. This equation for the fold-change is precisely what is plotted as a theory prediction in the top left pane of Figure 11(A).

#### 4.2. Beyond the Mean: Kinetic Treatments of Transcription

Up to this point, we have examined the simple repression architecture in a manner that describes the steady-state mean level of expression. But this is not to say that mRNA dynamics or the mRNA distribution are not of interest; quite the opposite. Knowledge of the higher moments of the distribution provide great insight into the kinetics of the system, and we turn to these now.

We begin by considering a dynamic description of repression that can be used to calculate the temporal evolution of the number of mRNA molecules as shown for the case of the constitutive promoter in

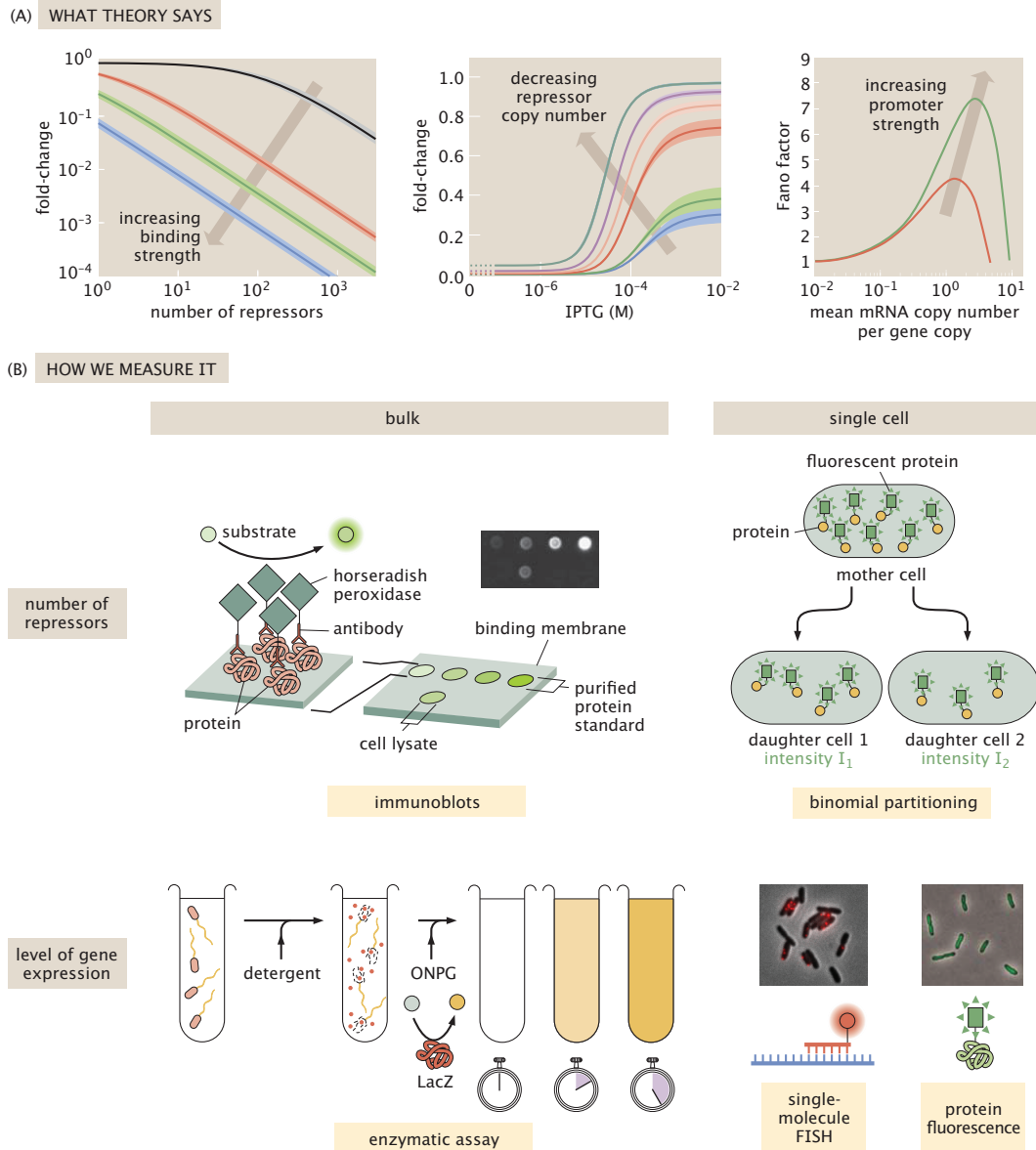


**Figure 11.** Theory/experiment dialogue in simple repression. (A) Three examples of predictions about the simple repression motif that can be subjected to experimental scrutiny using precision measurements. The left figure shows the fold-change in gene expression as a function of repressor copy number for different operators, the middle panel shows predictions of induction for different numbers of repressors and the right panel shows how gene expression noise (Fano factor = variance/mean) varies as a function of the mean gene expression level for different promoter strengths. (B) Bulk and single-cell measurements of both repressor copy number and gene expression. For copy number, bulk measurements can be done using immunoblotting, while counting statistics can be used at the single-cell level. To measure gene expression, bulk enzymatic assays have excellent dynamic range. Single-cell measurements can be done either by examining the level of mRNA or protein gene product.

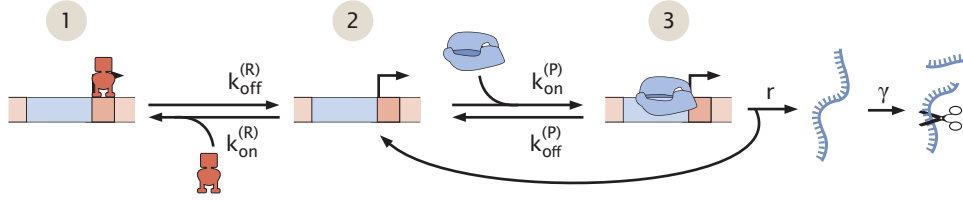


**Figure 12.** Kinetic model of simple repression. The promoter can be empty, occupied by repressor, or occupied by RNA polymerase. Transitions between the different states are characterized by rate constants shown in the caption. Note that when transcription commences from state 3, the promoter returns to the empty state (state 2).

Figure 9(B). Specifically, we think of simple repression using the kinetic scheme presented in Figure 12. For the kinetics of the first state, in which the promoter is occupied by the repressor molecule, the linear reaction scheme shows that there is only one way to enter and exit this state and that is through the “empty” state (state 2). This results in the dynamical equation

$$\frac{dp(1)}{dt} = k_{on}^{(R)} p(2) - k_{off}^{(R)} p(1). \quad (10)$$

The dynamics of the empty state (state 2) are more complicated because this state is accessible to both the repressor and the polymerase, meaning that the dynamics can be written as

$$\frac{dp(2)}{dt} = -k_{on}^{(R)} p(2) + k_{off}^{(R)} p(1) - k_{on}^{(P)} p(2) + k_{off}^{(P)} p(3) + rp(3). \quad (11)$$

Note that the final term in this equation reflects the fact that mRNA is produced at rate  $r$  from state 3 and once mRNA production begins, polymerase leaves the promoter and hence the system goes back to state 2. The state with polymerase occupying the promoter evolves similarly as can be seen by writing

$$\frac{dp(3)}{dt} = k_{on}^{(P)} p(2) - k_{off}^{(P)} p(3) - rp(3). \quad (12)$$

To close the loop and come full circle to the real question of interest, namely, the production of mRNA itself, we have

$$\frac{dm}{dt} = -\gamma m + rp(3). \quad (13)$$

What this equation tells us is that the promoter is only transcriptionally active in the third state, namely, that state in which the polymerase binds the promoter. The above equations can be solved in order to obtain the temporal dynamics of mRNA concentration, as we have illustrated in Figure 9(B) for the unregulated promoter.

An interesting feature of the kinetic description of simple repression presented here is that enables us to go beyond the steady-state and equilibrium assumptions that were invoked to calculate the fold-change in gene expression in Equations 8 and 9. Instead, we can use the kinetic scheme shown in Figure 12 to solve for the fold-change, but now only invoking steady-state by setting the left side in each equation above to zero. We begin by solving for the steady-state level of mRNA,  $m_{ss}$ , and find

$$m_{ss} = \frac{rp(3)}{\gamma}. \quad (14)$$

But what is  $p(3)$ ? In seeking the unknown steady-state probabilities, we must respect the constraint that the probabilities sum to one, namely,

$$p(1) + p(2) + p(3) = 1. \quad (15)$$

We will not go into the details of the algebra of resolving these three linear equations as these details are described in [43]. Instead, we will simply quote the result as

$$p(3) = \frac{1}{1 + \frac{(k_{off}^{(P)}+r)}{k_{on}^{(P)}} \left(1 + \frac{k_{on}^{(R)}}{k_{off}^{(R)}}\right)}, \quad (16)$$

which enables us to make contact with the types of experiments discussed earlier, by computing the fold-change:

$$\text{fold-change} = \frac{m_{ss}(R \neq 0)}{m_{ss}(R = 0)} = \frac{1}{1 + \frac{\frac{(k_{off}^{(P)}+r)}{k_{on}^{(P)}} \frac{k_{on}^{(R)}}{k_{off}^{(R)}}}{1 + \frac{(k_{off}^{(P)}+r)}{k_{on}^{(P)}} \frac{k_{on}^{(R)}}{k_{off}^{(R)}}}}. \quad (17)$$

Note that we can write  $k_{on}^{(R)} = k_+^{(R)} R$ , where we have acknowledged that the on-rate for the repressor is proportional to the number of repressors present in the cell. Interestingly, we see that this implies that the functional form of the fold-change is the same even in this steady-state context as it was in the thermodynamic model framework, though now at the price of having to introduce an effective  $K_d^{eff}$ , resulting in

$$\text{fold-change} = \frac{1}{\left(1 + \frac{R}{K_d^{eff}}\right)}. \quad (18)$$

By comparing Equations 9 and 18, we see that their scaling with repressor number is identical. To further explore the common features between these two expressions for fold-change, note that we can write

$$K_d^{eff} = \frac{k_{off}^{(R)} \left(1 + \frac{(k_{off}^{(P)}+r)}{k_{on}^{(P)}}\right)}{\frac{(k_{off}^{(P)}+r)}{k_{on}^{(P)}}}. \quad (19)$$

We can simplify this further by noting that we can write  $K_d^{(R)} = k_{off}^{(R)}/k_+^{(R)}$  resulting in

$$K_d^{eff} = K_d^{(R)} \frac{\left(1 + \frac{(k_{off}^{(P)}+r)}{k_{on}^{(P)}}\right)}{\frac{(k_{off}^{(P)}+r)}{k_{on}^{(P)}}}. \quad (20)$$

This equation reveals that the thermodynamic and kinetic treatments of simple repression have some interesting differences and clearly shows the consequences of imposing the equilibrium assumption in the thermodynamic calculation. The validity of this assumption will be explored in detail in Appendix 13.

An alternative way of viewing these same problems is by going beyond the description of the dynamics of the mean mRNA number and appealing to the kinetic theory of transcription in order to work out the time-evolution of the probabilities of the different states [45, 46, 47, 48, 49, 50, 51, 52]. Our goal is to write equations that describe the time evolution of the probability of finding  $m$  mRNA molecules at time  $t$ . This means that we need to define three coupled differential equations for the mRNA distribution in each of the three states, namely,  $p_1(m, t)$ ,  $p_2(m, t)$  and  $p_3(m, t)$ . Intuitively, if we are thinking about the possible changes that can alter state 1, there are only several transitions that can occur: i) the promoter can switch from state 1 to state 2, ii) the promoter can switch from state 2 to state 1 and iii) an mRNA molecule can decay resulting in a change in  $m$ . These transitions are expressed using the master equation formalism and the rate constants defined in Figure 12 as

$$\frac{dp_1(m, t)}{dt} = - \underbrace{k_{off}^{(R)} p_1(m, t)}_{(1) \rightarrow (2)} + \underbrace{k_{on}^{(R)} p_2(m, t)}_{(2) \rightarrow (1)} + \underbrace{\gamma(m+1) p_1(m+1, t)}_{m+1 \rightarrow m} - \underbrace{\gamma m p_1(m, t)}_{m \rightarrow m-1}. \quad (21)$$



The case of state 2 includes the same transitions between state 1 and state 2, as well as the transitions between state 2 and 3 as a result of polymerase unbinding or promoter escape due to transcriptional initiation. Incorporating these ideas leads to an equation of the form

$$\begin{aligned} \frac{dp_2(m, t)}{dt} = & \underbrace{k_{off}^{(R)} p_1(m, t)}_{(1) \rightarrow (2)} - \underbrace{k_{on}^{(R)} p_2(m, t)}_{(2) \rightarrow (1)} + \underbrace{k_{off}^{(P)} p_3(m, t)}_{(3) \rightarrow (2)} - \underbrace{k_{on}^{(P)} p_2(m, t)}_{(2) \rightarrow (3)} + \underbrace{r p_3(m-1, t)}_{\substack{m-1 \rightarrow m \\ (3) \rightarrow (2)}} \\ & + \underbrace{\gamma(m+1) p_2(m+1, t)}_{m+1 \rightarrow m} - \underbrace{\gamma m p_2(m, t)}_{m \rightarrow m-1}. \end{aligned} \quad (22)$$

Finally for state 3 we must account for the transitions between state 2 and state 3, and the mRNA production at a rate  $r$ . Bringing all of these transitions together results in

$$\frac{dp_3(m, t)}{dt} = - \underbrace{k_{off}^{(P)} p_3(m, t)}_{(3) \rightarrow (2)} + \underbrace{k_{on}^{(P)} p_2(m, t)}_{(2) \rightarrow (3)} - \underbrace{r p_3(m, t)}_{\substack{m \rightarrow m+1 \\ (3) \rightarrow (2)}} + \underbrace{\gamma(m+1) p_3(m+1, t)}_{m+1 \rightarrow m} - \underbrace{\gamma m p_3(m, t)}_{m \rightarrow m-1}. \quad (23)$$

This set of coupled equations describes the time evolution of the probability distribution  $p(m, t)$ .

As described in the following sections, the equations written above imply a steady-state mRNA distribution that can be used to compute both the mean and variance in gene expression. In order to render the different theoretical descriptions self-consistent, the thermodynamic parameters such as the repressor binding energy  $\Delta\varepsilon_R$  must constrain the values that the repressor rates  $k_{off}^{(R)}$  and  $k_{on}^{(R)}$  can take. Now that we have seen how theory can be used to sharpen our thinking, we turn to how experiments can be designed to test those theoretical ideas.

## 5. “Spectroscopy” for the Simple Repression Hydrogen Atom: Precision Measurements on Gene Expression

Figure 11 provides a picture of how theory and experiment come together in thinking about the simple repression motif. As part (B) of that figure shows, there are a variety of approaches that can be taken to count the repressors and to measure the level of gene expression. Expression levels can be quantified using enzymatic or fluorescence assays. Note that by choosing to measure the ratio of level of gene expression (i.e. the fold-change) rather than the absolute value of the gene expression itself, the system is further simplified since various categories of context dependence such as the position of the gene on the genome are normalized away. This is not to say that the description of such effects on the absolute level of expression are uninteresting, but rather the focus on a predictive understanding of the fold-change in gene expression reflects the spirit of little steps for little feet that are required to progressively develop a rigorous view of these problems.

There are many facets to the regulatory response of the simple repression motif that can be subjected to experimental scrutiny in order to compare them to the results of theoretical predictions, as shown in Figure 11(A). Indeed, the seeds of this review were planted by many wonderful earlier works that explored various aspects of the theoretical and experimental strategies laid out in Figure 11. Experimentally, as noted above, Muller-Hill and Oehler led the way in the *lac* system (see Figure 8) as did Schleif in the context of the arabinose operon [53, 54, 55]. On the theory side, Ackers and Shea laid the groundwork for thermodynamic models which allow us to predict the mean level of expression [35, 36]. These models were pushed even further by Buchler, Gerland and Hwa [37] and by Vilar, Saiz and Leibler [38, 39, 56]. Besides the thermodynamic model approach [34, 40, 41, 42], others have been interested in gene expression noise, which demands kinetic models. These approaches to transcription have offered numerous insights of their own [45, 46, 47, 48, 49, 52]. Much of the work presented here draws inspiration from modern

quantitative dissections of the wild-type *lac* operon [57, 16], as well as from efforts that made it possible to measure gene regulatory functions at the single cell level [58, 59], and from research that embodies the same interplay between theory and experiment featured in this article but in the context of other gene-regulatory architectures [60, 61, 62, 63].

## 6. Climbing the Simple Repression Pyramid: A Minimal Parameter Set to Rule Them All

In the previous sections we outlined how different kinds of theoretical frameworks enable us to formalizing our “pathetic thinking” in order to refine our prejudices about how a complex system behaves [64]. One of the key requirements we insist on in using such theoretical frameworks to describe simple repression is that a single set of parameters applies across all different situations, as illustrated in Figure 11. There is a long tradition of developing phenomenological theories that describe broad classes of behaviors, in which the underlying microscopic processes that give rise to material response are captured in the form of a small set of phenomenological, but measurable, parameters. Consider the steel used to build our bridges and skyscrapers, or the aluminum used to build our airplane wings: several elastic constants, a yield stress and a fracture toughness often suffice to fully characterize the material response under a broad array of geometries and loading conditions [65]. Importantly, each time we go out and use those materials for something new, we don’t have to introduce a new set of parameters. It is critical to realize that there is no requirement whatsoever for an underlying “mechanistic theory” of what determines those parameters in order for a phenomenological theory to be both beautiful and far-reaching in its predictive value. Though perhaps the “microscopic mechanism” of, for example, how the interactions between the nucleotides on the DNA and residues on the repressor dictate binding energy is attractive to some investigators, we do not need a microscopic understanding of these atomic-level “mechanisms” to construct a predictive theory of gene regulation. Indeed, though much progress has been made in constructing a microscopic basis for these parameters, we generally cannot predict these material parameters from first principles.

Here, we adopt a phenomenological mindset in the context of the gene regulatory response. Though it is clear that there are a huge variety of complicated processes taking place within the cell that we do not understand, we address whether it is nonetheless possible to introduce a few key effective parameters that will allow us to characterize the regulatory response of the simple repression motif under a broad array of different circumstances. Figure 13(A) shows us how the theoretical ideas highlighted in the previous sections demand a small number of parameters before we can use them predictively. For example, in the simple repression motif, we require a binding energy  $\Delta\varepsilon_R$  (or equivalently a  $K_R$ ) to characterize the strength of repressor binding to operator. Similarly, when describing the induction response of transcription factors to inducer, we require parameters  $K_A$  and  $K_I$  that describe the affinity of inducer to the transcription factor when it is in its active and inactive states, respectively [66]. We also require a free energy difference  $\Delta\varepsilon_{AI}$  that characterizes the relative stability of the active and inactive states in the absence of inducer. Finally, when describing gene expression dynamics, we require rate constants for mRNA degradation ( $\gamma$ ), transcript initiation ( $r$ ), and the on and off rates of repressor and RNA polymerase to their binding sites ( $k_{on}^{(R)}$  and  $k_{off}^{(R)}$  for the repressor, and  $k_{on}^{(P)}$  and  $k_{off}^{(P)}$  for RNA polymerase). The question we ask is: once we have established this minimal set of parameters, how well can we then range in our predictions across different classes of experiments involving the simple repression motif?

We now show how it is possible to ascend the simple repression pyramid introduced in Figure 3. In Figure 13(B), we outline how we fully determined a single minimal set of parameters needed to characterize a host of regulatory responses. Note that others have also made complete parameter determinations, but did so across different experiments [17]. The lefthand panel of Figure 13(B) illustrates how experiments like those of Oehler *et al.*, with one particular repressor copy number and a specific operator sequence, can be used to determine the parameter  $\Delta\varepsilon_R$  (or  $K_R$ ). The second experiment highlighted in Figure 13(B) shows how the transcription factor titration effect can be used to determine the parameter  $\Delta\varepsilon_{AI}$  (or

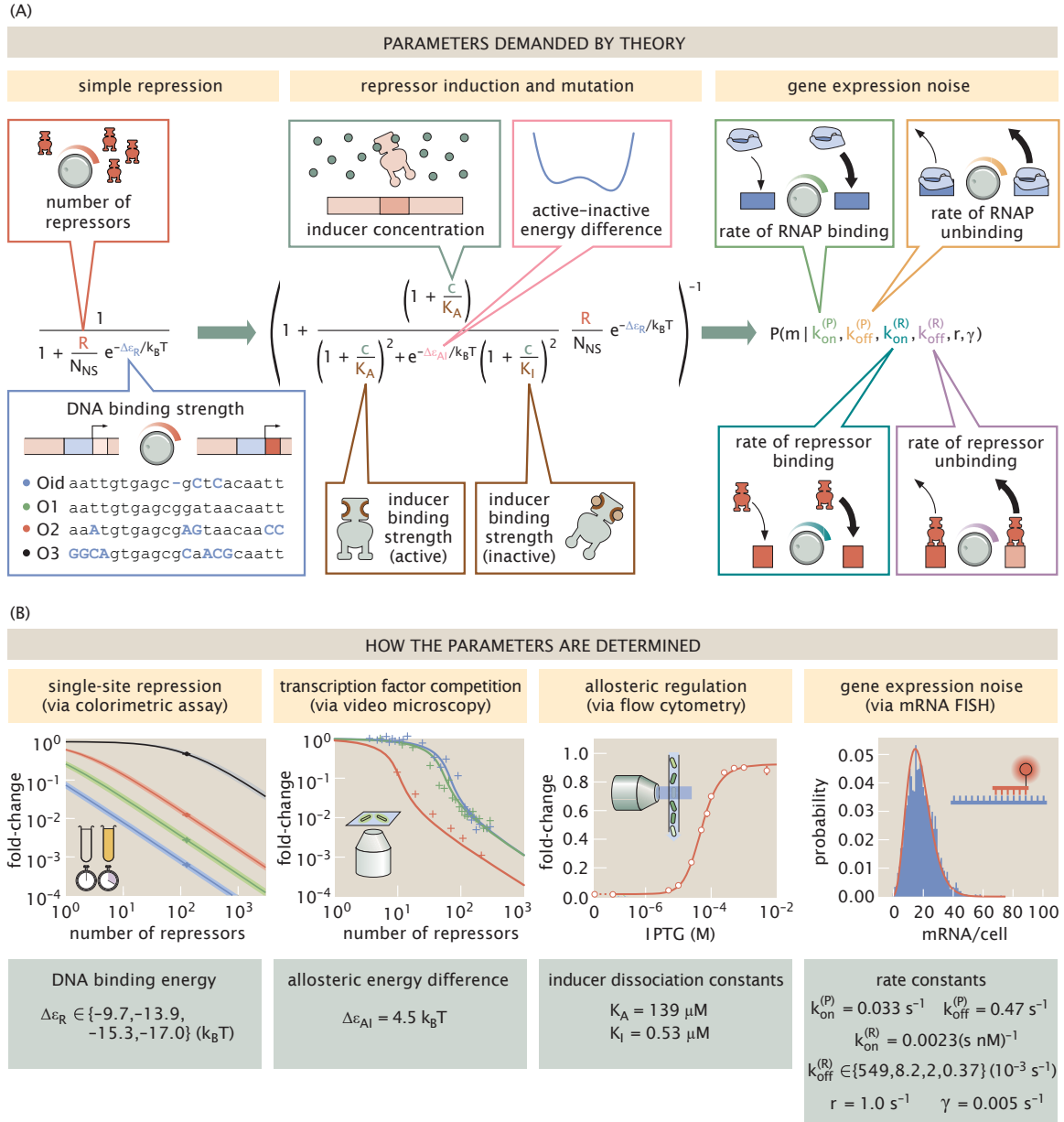


**Figure 13.** Determination of the minimal parameter set for describing simple repression across a broad array of experimental approaches and simple repression regulatory scenarios. (A) Parameters that are introduced in the description of simple repression fold-change measurements, induction experiments and in the context of gene expression noise. (B) Experiments used to determine the minimal parameter set. (B, left panel adapted from [44], middle panels adapted from [66], right panel adapted from [67])

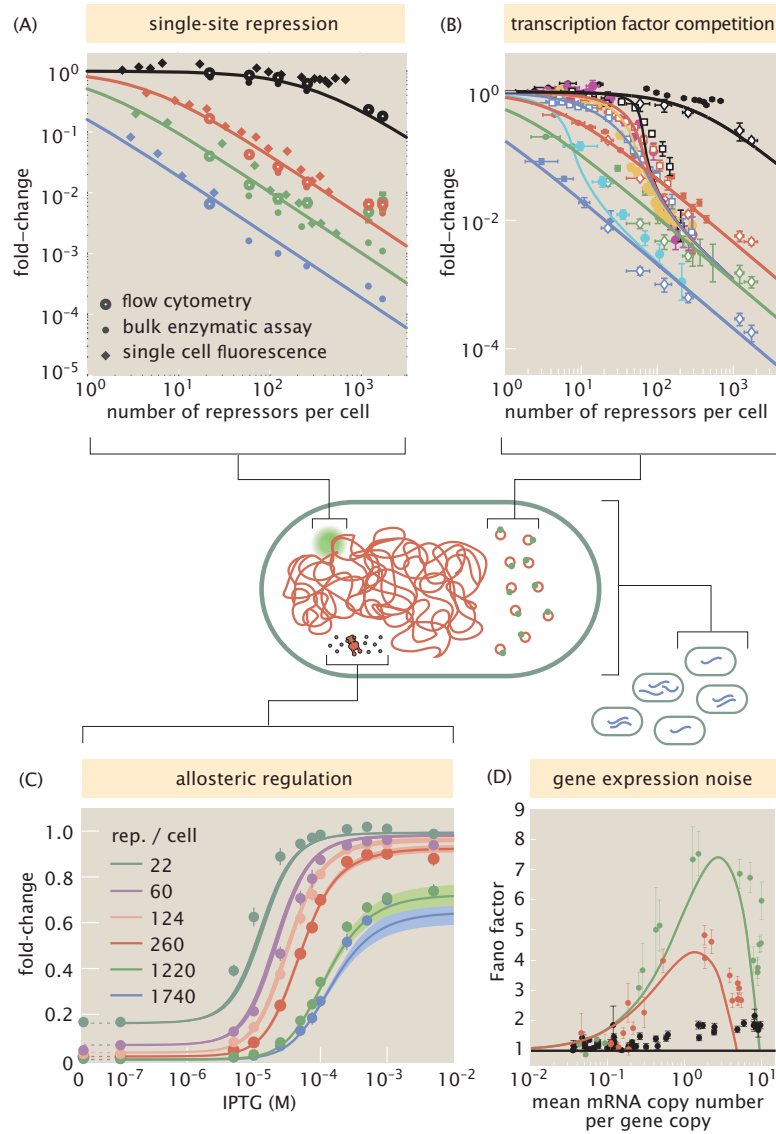
alternatively  $L = e^{-\beta\Delta\epsilon_{AI}}$ ) which characterizes the equilibrium between the inactive and active states of repressor in the absence of inducer. The third panel in the figure shows how a single induction response curve can fix the parameters  $K_A$  and  $K_I$  that determine the binding of inducer to the repressor in the active and inactive states, respectively. Finally, the righthand panel demonstrates how, by going beyond the mean and looking at the full mRNA distributions for the constitutive promoter and the simple repression motif, it is possible to infer the rates of RNA polymerase and Lac repressor binding and unbinding as well as the rates of mRNA production and degradation.

This kinetic approach takes advantage of the known closed form of the full mRNA distribution for a two-state promoter [46]. Using this expression for the distribution we can perform a Bayesian parameter inference to obtain values for the polymerase rates  $k_{on}^{(P)}$  and  $k_{off}^{(P)}$ , as well as for the mRNA production rate  $r$  that fit the single molecule mRNA count data from [67]. The kinetic rates for the repressor are obtained by assuming that  $k_{on}^{(R)}$  is diffusion-limited [67], and demanding that  $k_{off}^{(R)}$  be consistent with the binding energies obtained in the lefthand panel of Figure 13(B). We note, however, that this model differs from the one presented in Figure 12 in the sense that upon initiation of transcription at a rate  $r$ , the system does not transition from state 3 to state 2. Further comparison between this model and the model presented in Figure 12 is still needed and will be explored in future work [68].

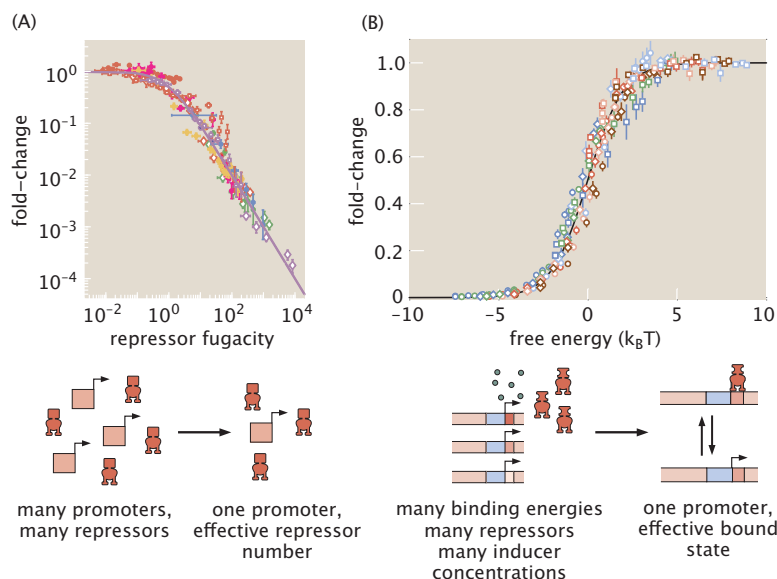
With our single minimal parameter set in hand, it is now time to take the leap and to see whether the theoretical framework that has been used to describe various facets of the simple repression architecture actually works. Figure 14 shows the diversity of predictions and corresponding measurements that partner with the predictions given at the top of Figure 11. In fact, the understanding summarized in this figure was developed sequentially rather than with the “all at once” appearance conjured up by Figure 13. Indeed, that is the principal reason that the discussion is so self-referential since over the last decade, inspired by the many successes of others [33, 69, 38, 15, 16, 17], we undertook a systematic effort to design experiments that allowed us to control the various knobs of transcription already highlighted, to construct the strains that make this possible and then to do the highest precision measurements we could in order to test these predictions.

Figure 14(A) shows a modern and predictive incarnation of the experiments done by Oehler *et al.* to determine the response of the simple repression motif to changes in repressor numbers and operator sequence (we showcased their results earlier in Figure 8). In this set of experiments, our ambition was to control both the copy number of repressors and operator binding strengths and systematically measure the resultant expression over the entire suite of different constructs, using only one repressor copy number for each DNA binding strength to determine the parameter  $\Delta\epsilon_R$  as described above. The measurements were taken in multiple ways: we used both enzymatic and fluorescent reporters to read out the level of gene expression, and we separately counted the number of repressors using quantitative immunoblotting and fluorescence measurements. One of our central interests is in whether or not different experimental approaches to ostensibly identical measurements yield the same outcomes. We were encouraged, at least in this case, to find reasonable concordance between them.

The level of expression from our simple repression promoter can be significantly affected if the repressors are enticed away from it by other binding sites. The results of this much more demanding set of predictions surrounding the transcription factor titration effect [70] are shown in the next panel of the figure, Figure 14(B). There are a number of ways to titrate away repressors: we can put extra copies of our gene of interest on the chromosome or on plasmids (shown in the schematic below the data), or use plasmids to simply introduce decoy binding sites for the repressor that have no explicit regulatory role other than pulling it out of circulation, effectively tuning the chemical potential of the repressor. Note that in this case, the fold-change has a particularly rich behavior and this is on a log-log plot, where functional forms often appear as straight lines. Figure 15(A) brings together all of the data from Figure 14(A) and (B) under one simple conceptual roof by determining the natural scaling variable of the simple repression motif. This data collapse implies that any combination of repressor concentration, binding site strength, and number and strength of competing binding sites can be replaced by an equivalent effective promoter



**Figure 14.** Experiment-theory dialogue in simple repression. All curves are parameter-free predictions based upon the minimal parameter set introduced in Figure 13. (A) Fold-change for simple repression as a function of repressor copy number and operator strength for a single gene copy [44, 70]. (B) Fold-change for simple repression as a function of repressor copy number and operator strength with repressor titration effect [70]. (C) Induction of the simple repression motif for different numbers of copies of the repressor [66]. (D) Measurement of gene expression noise for simple repression motif as reported by the Fano factor (variance/mean) [67].



**Figure 15.** Data collapse of all data from the simple repression architecture. (A) Gene expression in the simple repression motif is dictated by an effective repressor copy number [72]. (B) Level of induction depends upon inducer concentration, repressor copy number and repressor binding strength all of which fold into the free energy difference between active and inactive forms of the repressor [66].

consisting of one binding site and an effective repressor number.

The middle panel of Figure 11(A) highlights the next level in the hierarchy of theoretical predictions that can be made about the simple repression motif, namely, how this motif responds to inducer. In Figure 14(C) we show one example (from a much larger set of predictions [66]) of how the induction response can be predicted for different operator strengths and repressor copy numbers. Here we highlight predictions for the *O2* operator ranging over the same repressor copy numbers already shown in Figure 14(A). As with our ability to introduce the natural variables of the problem in Figure 15(A), induction responses also have a scaling form that permits us to collapse all data onto a single curve (Figure 15(B)). Once again, the emergence of this natural scaling variable tells us that any set of repressor number, binding energies and inducer concentrations can be mapped onto a simple repression architecture with a corresponding effective binding energy.

The final part of our comparison of theory and experiment in the context of the simple repression motif is shown in Figure 14(D). The predictions about gene expression noise were already highlighted in the right panel of Figure 11(A). Here what we see is that the Fano factor (i.e. the variance normalized by the mean) is quite different for constitutive promoters and promoters subject to repression in the simple repression motif [67]. Discrepancies between the noise revealed in different regulatory architectures remain to be resolved [71].

The hierarchical analysis presented in Figure 14 illustrates the unity of outlook and parameters afforded by performing all experiments in the same strains. When experimental consistency is placed front and center, one minimal set of parameters appears to serve as a predictive foundation for thinking about a broad variety of different constructs and conditions over a host of different experimental scenarios and methods.

Nearly fifty years ago, Theodosius Dobzhansky wrote a beautiful article in *American Biology Teacher* entitled “Nothing in biology makes sense except in the light of evolution” [73]. This phrase, now an oft-quoted tenet of modern biology, has resulted in evolution as the capstone to numerous biological pyramids. As such, there is a reason we talk about *climbing* the simple repression pyramid rather than

saying that *we have climbed* it. Though the evolutionary aspects of transcription are represented by the smallest part of the pyramid in Figure 3, they are perhaps the most daunting. At the time of writing, many different groups are still working to construct this section of the pyramid for simple repression [74, 75, 76, 77, 78, 79].

To make meaningful predictions about the evolutionary potential of the simple repression motif, it is a requirement that we have a thorough knowledge of the minimal parameter set described in the preceding section. For example, we have shown that the sequence of the operator strongly influences the maximum level of gene expression given an input such as the concentration of inducer. One could extend this conclusion to make predictions of how the various properties of the induction profiles could change due to mutation. It is reasonable to assume that mutations in the DNA binding pocket would alter only the strength of DNA binding and leave the inducer binding constants the same as the wild type. Conversely, mutations in the inducer binding domain would alter only the inducer binding constants. With quantitative knowledge of the single mutants, the theoretical underpinnings allow us to assume a naïve hypothesis in which the two mutations are additive, resulting in a predictable change in the induction profile. Measurements of this flavor have been performed and published [80], however without knowledge of the parameters, the predictive power is extremely limited.

## 7. A Critical Analysis of Theories of Transcription

Thus far, we have painted a rosy picture of the dialogue between theory and experiment in the study of transcription in the simple repression motif. It is now time to critique these approaches and see what such critiques imply about future efforts to dissect the regulatory genome. In the paragraphs that follow, we have amassed a series of worthy critiques of the program laid out thus far in the paper, and in each case, we set ourselves the task of sizing up these critiques to see what we can learn from them. Our strategy is to discuss the high points of the analysis in the main body of the text and to relegate the technical details behind that analysis to the appendices.

*The Equilibrium Assumption in Thermodynamic Models.* As already seen in Figure 9, there are multiple approaches to modeling transcription. One broad class of models sometimes goes under the heading of “thermodynamic models”, but we would rather refer to them as models founded upon the *occupancy hypothesis*. We can examine two critical questions about such models, shown diagrammatically in Figure 16(A): (i) to what extent is it true that the rate of transcription is proportional to the probability of promoter occupancy and (ii) can promoter occupancy be fruitfully computed using the quasi-equilibrium assumption?

Recall that the assumption that the rate of transcription is proportional to the probability of RNA polymerase binding to the promoter is central to the thermodynamic models. Indeed, this assumption makes it possible to connect a theoretically accessible quantity,  $p_{bound}$ , to an experimentally measurable quantity,  $dm/dt$ . This connection can be used to test the predictions stemming from these models. To answer the question of whether the rate of transcription is proportional to  $p_{bound}$ , we must remember that, as shown in Figure 16(A), there is a plethora of kinetic steps between the binding of RNA polymerase and transcription factors to the DNA, and the ultimate production of an mRNA molecule. Further, steps such as “initiation” in the figure are an oversimplification, as the process leading to promoter clearance and the initiation of productive transcription is composed of multiple intermediate steps [47]. In Appendix 11 we explore the conditions under which this occupancy hypothesis is fulfilled. In particular, we consider a situation where the transition rates between intermediate steps correspond to zero-order reactions. To illustrate this, we refer to the first transition in Figure 16(A), which shows that the fraction of RNA polymerase molecules initiating transcription, denoted by  $I$ , is related to  $p_{bound}$ . In a zero-order reaction scheme, the temporal evolution of  $I$  is given by

$$\frac{dI}{dt} = r_i p_{bound}, \quad (24)$$

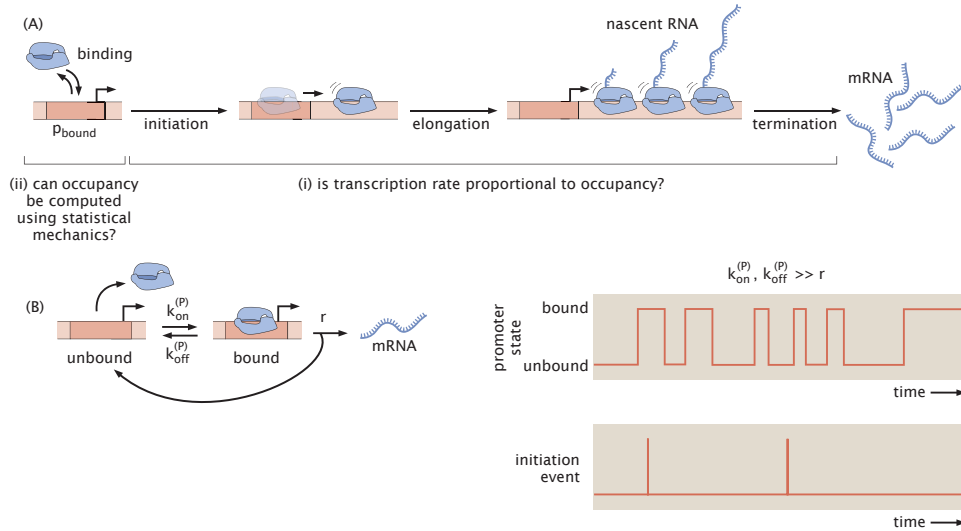


**Figure 16.** The occupancy hypothesis and the equilibrium assumption. (A) The multiple steps between RNA polymerase binding and the termination of an mRNA raise the question of whether the binding probability (occupancy) of RNA polymerase to the promoter can be used as a proxy for the quantity of mRNA produced, and whether RNA polymerase binding is in quasi-equilibrium such that the tools of statistical mechanics can be used to compute this quantity. (B) The equilibrium assumption is fulfilled if the rates of RNA polymerase binding and unbinding ( $k_{on}^{(P)}$  and  $k_{off}^{(P)}$ , respectively) are much faster than the rate of transcriptional initiation  $r$ . See Appendix 13 for details on this simulation.

where  $r_i$  is the rate of transcriptional initiation. In this scenario, the rate of change in the fraction of molecules initiating transcription is proportional to the fraction of molecules bound to the promoter. As described in the Appendix, under this assumption, Equation 1 can be used to relate the probability of finding RNA polymerase bound to the promoter to the rate of mRNA production.

Putting the occupancy hypothesis to a direct and stringent test requires us to have the ability to simultaneously measure RNA polymerase promoter occupancy and output transcriptional activity. The development of new approaches to directly measure DNA-binding protein occupancy in the vicinity of a promoter and relate this binding to output transcriptional activity will make it possible to realize such a test in the near future [81, 82, 83, 84]. While technology catches up to the demands of our theoretical models, an indirect strategy for testing the occupancy hypothesis is to simply ask how well the thermodynamic models do for the various predictions highlighted throughout the paper. Figure 14 suggests that, for the *lac* operon, the occupancy hypothesis is valid. However, it is important to note that there are cases where this hypothesis has been explicitly called into question both in the *lac* operon [85, 82] and other regulatory contexts [86, 87]. As a result, the validity of the occupancy hypothesis should be critically examined on a system-by-system basis.

The second key assumption to be considered is the extent to which the system can be viewed as being in “equilibrium”, such that the tools of statistical mechanics can be applied to calculate  $p_{bound}$  and the fold-change. This equilibrium assumption permeates the vast majority of the work presented here. In Appendix 13 we dissect it in the context of the kinetic rates revealed in Figure 13(B). As we showed in Figure 16(B), in order for equilibrium to be a valid assumption when calculating  $p_{bound}$  for the constitutive promoter, the rates of RNA polymerase binding and unbinding ( $k_{on}^{(P)}$  and  $k_{off}^{(P)}$ , respectively) need to be much larger than the rate of initiation  $r$ . However, we find that the inferred rates do not justify the use of the equilibrium assumption: the rate of RNA polymerase unbinding from the promoter is not much faster than the subsequent rate of initiation, such that the system does not get to cycle through its various binding states and equilibrate before a transcript is produced. However, our calculations reveal



that, given these same rates, the fold-change in gene expression can be calculated based on the equilibrium assumption. As discussed in detail in the Appendix, if  $k_{on}^{(P)} \ll k_{off}^{(P)} + r$ , then when the system transitions to the polymerase-bound state, it will quickly revert back to the unbound state either by unbinding or through transcription initiation. As a result of this separation of times scales, the repressor gets to explore the bound and unbound states such that its binding is equilibrated even if the RNA polymerase binding is not.

Finally, it is important to note that our conclusions about the applicability of equilibrium rely on committing to the kinetic scheme presented in Figure 12 and on the inferred parameters shown in Figure 13(B). Changes to the molecular picture of the processes underlying repression and gene expression could significantly affect our conclusions. Indeed, researchers have cast doubt on the applicability of equilibrium to describe the *lac* operon [82] as well as other gene-regulatory systems [88, 89].

*Reconciling Thermodynamic Models and Statistical Mechanical Models.* Thermodynamic models of transcription can be formulated either directly in the language of statistical mechanics, by invoking binding energies and explicitly acknowledging the various microscopic states available to the system, or in the language of thermodynamics, in which DNA-protein interactions are characterized using dissociation constants. The literature is not always clear about the relation between these two perspectives and our central argument (fleshed out in detail in Appendix 12) is that they are equivalent. That argument was really already made in Figure 10, in which we saw that the statistical weights of the three states of the simple repression motif can be written in either of these languages.

We personally favor the statistical mechanical language because we find that, in going to new regulatory architectures, it is more microscopically transparent to enumerate the microscopic states and their corresponding energies than to invoke dissociation constants that combine these microscopic interactions into an effective parameter as shown below for the case of the nonspecific background. One related point of possible confusion concerns the use of parameters such as  $N_{NS}$  in the statistical mechanical approach to occupancy models of transcriptional regulation. In the Appendix, we demonstrate that the dissociation constant  $K_d$  is given by

$$K_d = \frac{N_{NS}}{V_{cell}} e^{-\beta \Delta \varepsilon}. \quad (25)$$

This equivalence shows that the parameter  $N_{NS}$ , which reflects the genome size and hence the size of the nonspecific background binding landscape, is in fact just a contribution to the standard state concentration used in conjunction with the dissociation constant  $K_d$  in disguise.

*The Energy of Nonspecific Binding.* One of the key simplifying assumptions often invoked in the context of thermodynamic models of transcription is the treatment of the binding of transcription factors to the nonspecific background as though all such nonspecific sites are equivalent. For transcription factors such as LacI, there is wide-ranging evidence from diverse types of experiments (e.g. measurements of the protein content of genome-free mini-cells and imaging using modern microscopy techniques) that these transcription factors are almost always bound to the genome rather than free in cytoplasm [90, 91, 92]. As such, when computing the probability of promoter occupancy by either polymerase or repressors, we need to account for the distribution of these molecules across the remainder of the genome.

With an approximately  $5 \times 10^6$  basepair genome as in *E. coli*, it at first blush seems ridiculous to proceed as though  $5 \times 10^6 - 1$  of those sites have the exact same energy,  $\varepsilon_{NS}$ . To explore the distribution of nonspecific energies, one idea is to slide an energy matrix, much like those determined through Sort-Seq [93, 94, 95, 96], across the entire genome, base pair by base pair, to get the full distribution. Such a distribution is shown in Figure 17 where the energy matrix for the LacI repressor was applied to the entire *E. coli* genome. We see immediately that an exceedingly small number of sites have a negative binding energy, meaning more preferable binding than the vast majority of sites, which are found to be positive. The three native *lac* operators, shown as black, red, and green vertical lines, have highly negative binding energies compared to the rest of the sites. With knowledge of the distribution, it is tempting to use this directly in the thermodynamic calculations to possibly get a better treatment of the

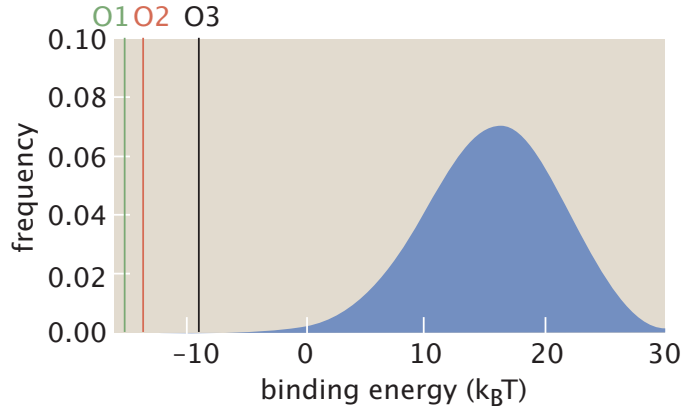


**Figure 17.** Distribution of nonspecific binding energies. The distribution shows the predicted binding energies for LacI to all possible 21 bp sequences on the *E. coli* genome (strain MG1655, GenBank: U00096.3). Binding energies were calculated using an energy matrix obtained by Sort-Seq on the LacI simple repression architecture [99].

nonspecific background. However, for now, it is a luxury to have an accurate energy matrix that reports the binding energy of a given transcription factor to a DNA binding site *in vivo*. We certainly don't know the binding energy matrix for all transcription factors that would permit the determination of the distribution of nonspecific binding energies.

But more interestingly, as we show in detail in Appendix 14, there really is no difference between using the complete distribution of binding energies versus an effective energy of the entire genome. This concept is explored in detail in the Appendix and agrees with more sophisticated treatments using concepts from statistical physics [97, 98]. We treat this problem using the three toy models shown in Figure 26. First, we assume that there is a uniform binding energy distribution in which all binding sites have the same energy. By definition, this is the simplest approach where this energy can be used directly in the partition function. The second example is the extreme case in which there are only two nonspecific binding energies,  $\epsilon_1$  and  $\epsilon_2$ , which are evenly distributed about the genome. In this case we can show the nonspecific background behaves as though it has a single effective binding energy of the form

$$\epsilon_{NS} = \frac{\epsilon_1 - \epsilon_2}{2}, \quad (26)$$

showing that the effective nonspecific binding energy  $\epsilon_{NS}$  tells the exact same story as using the full distribution. Finally, we take the more realistic case in which we assume a Gaussian distribution of binding energies across the genome with mean  $\bar{\epsilon}$  and standard deviation  $\sigma$ , much like what is seen in Figure 17. Here, a few more mathematical steps outlined in the Appendix delivers us to the result,

$$\epsilon_{eff.} = \bar{\epsilon} - \frac{\beta\sigma^2}{2}. \quad (27)$$

Note that this shows that even if we have a Gaussian distribution of nonspecific binding energies, it can be treated exactly as a uniform distribution with a single effective energy.

*Promoter competition against nonspecific DNA-binding proteins.* Up until this point, we have considered the effect of LacI nonspecific binding throughout the genome on its regulatory action in the context of the simple repression motif. However, just like in the simple repression motif where the promoter and operator constitute the specific binding sites for RNA polymerase and repressor, respectively, these same sequences serve as substrates for the nonspecific binding of other DNA-binding proteins that decorate the bacterial genome. In Appendix 15, we show how the effect of these nonspecific competitors can

be absorbed into an effective number of nonspecific binding sites  $N_{NS}$  such that the theoretical models describing the simple repression motif retain their predictive power. Interestingly, the calculations presented in the Appendix also suggest that, as the concentrations of these DNA-binding proteins is modulated due to changes in growth rate, the effect of these competitors on the rescaled  $N_{NS}$  remains unaltered. This indifference to growth rate stems from the fact that, as growth rate increases, both the overall protein concentration and the cell’s DNA content increase. This simultaneous increase in protein and DNA concentration leads to a relatively constant number of proteins per DNA target in the cell irrespectively of growth conditions.

*Is Gene Expression in Steady State?* A critical assumption in our experimental measurements of gene expression is that gene expression is in steady-state. The definition of steady-state has different meanings depending on the method of measurement. For mRNA FISH, for example, we assume that the mRNAs are produced at rate  $r$  that matches the rate of degradation  $\gamma m_{ss}$ , where  $m_{ss}$  is the steady-state level of mRNA. When measuring protein expression, we assume that the protein accrued over the cell cycle is negated by the dilution of these proteins into the daughter cells upon division, as is shown in Figure 18(A). Through this assumption, we are able to state that, on average, a single measurement represents the level of expression for that particular time point rather than integrating over the entire life history of the cell. A typical rule-of-thumb is that steady-state expression is reached when the cells enter the exponential phase of growth.

We put this hypothesis to the test by directly measuring the expression level of exponential phase *E. coli* over time. Using video microscopy, we monitored the growth of cells constitutively expressing YFP in exponential phase ( $OD_{600nm} \sim 0.3 - 0.4$ ) in minimal medium with a doubling time of approximately an hour (Figure 18(A)) following the experimental approach undertaken by Brewster *et al.* [70]. Starting from a single cell, we tracked the lineages as the microcolony developed and compared the fluorescence in arbitrary units of each cell to the founding mother cell. If steady-state gene expression has been achieved, this approach, schematized in Figure 18(B), will result in an average difference in fluorescence  $\Delta I$  of zero. The results of this experiment are shown in Figure 18(C). In the figure, we see that individual measurements (red points) are scattered about zero but that, once the mean difference in intensity is considered (blue triangles), the data becomes very tightly distributed about zero (black dashed line). These results show that, when cells are growing in exponential phase, gene expression levels are in steady-state and the reporter is not accrued over the life history of the cell lineage.

*Allosteric Models vs Hill Functions.* Though many thermodynamic models of gene regulation attempt to enumerate the entirety of microscopic states and assign them their appropriate statistical weights, it is also extremely popular to adopt a strictly phenomenological model of binding described by Hill functions. It is undeniable that the Hill function features prominently in the analysis of many biological processes (for interesting examples see, [100, 101, 57, 78]). However, treating allosteric systems with Hill functions often abstracts away the important physical meaning of the parameters and replaces them with combinations of polynomials often referred to as “lumped parameters”. For example, one could treat the induction profiles of LacI discussed earlier in this work using a Hill equation of the form,

$$\text{fold-change} = \text{leakiness} + \text{dynamic range} \frac{\left(\frac{c}{K_D}\right)^n}{1 + \left(\frac{c}{K_D}\right)^n}, \quad (28)$$

where the leakiness is set as the zero point of expression. With increasing concentration  $c$  of ligand, the leakiness is modified by an expression describing the activity of the repressor using a Hill function. In this expression,  $c$  corresponds to the concentration of inducer.  $n$  is the Hill coefficient which describes the cooperativity of repression, and  $K_D$  is an effective dissociation constant [16].

Note that nowhere in this expression is any treatment of the allosteric nature of the protein! While structural biology has demonstrated that this repressor can exist in active and inactive states, each of which has its own dissociation constant for the inducer, all of these details have been lumped into the  $K_D$

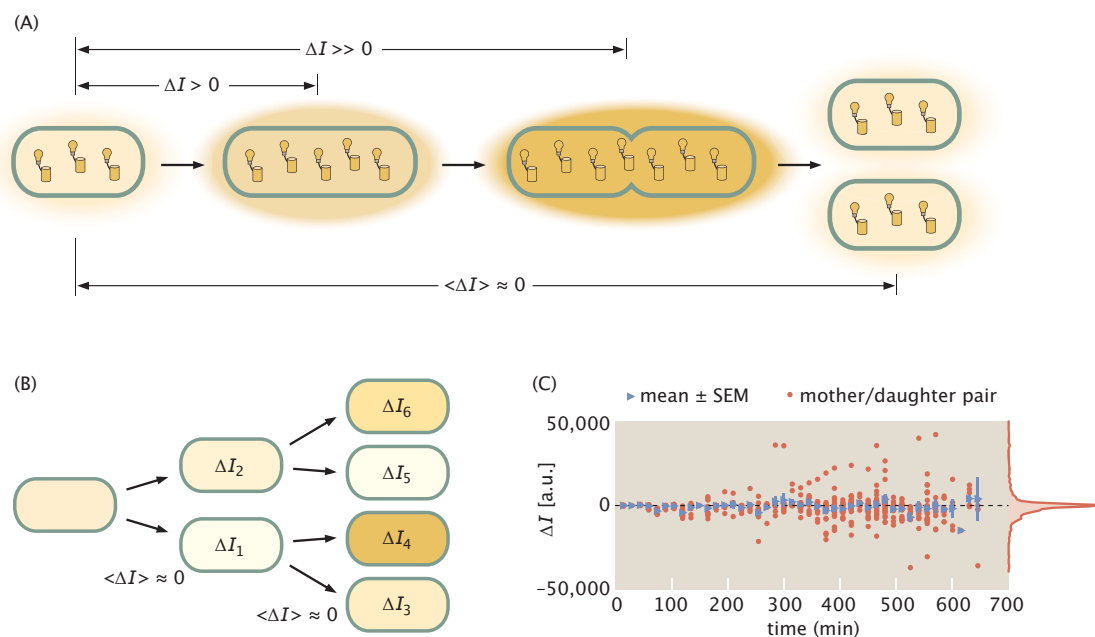


**Figure 18.** Test of the idea of steady-state gene expression for cells in exponential phase. (A) Diagrammatic view of protein dilution through cell division. As cells grow, the expression of fluorescent proteins marches on. As the cell approaches division, the total detected fluorescence is much larger than detected at the cells' birth. On average, the proteins are split evenly among the daughter cells, resulting in a comparable fluorescence level as the original mother cell. (B) Schematic of experimental measurement. To test the steady-state hypothesis, we monitored the growth of several bacterial microcolonies originating from single cells and tracked the difference in intensity with respect to their mother cell as a function of time for each daughter cell through the family tree. (C) Fluorescence intensity difference between mother/daughter pairs as a function of time. Red points indicated individual daughter/mother pairings in a given lineage. Blue triangles represent the average difference at that time point. Error bars on blue points are the standard error of the mean. A kernel density estimation of the  $\Delta I$  distribution is shown on the right-hand side of the plot. The black dashed line is at zero.

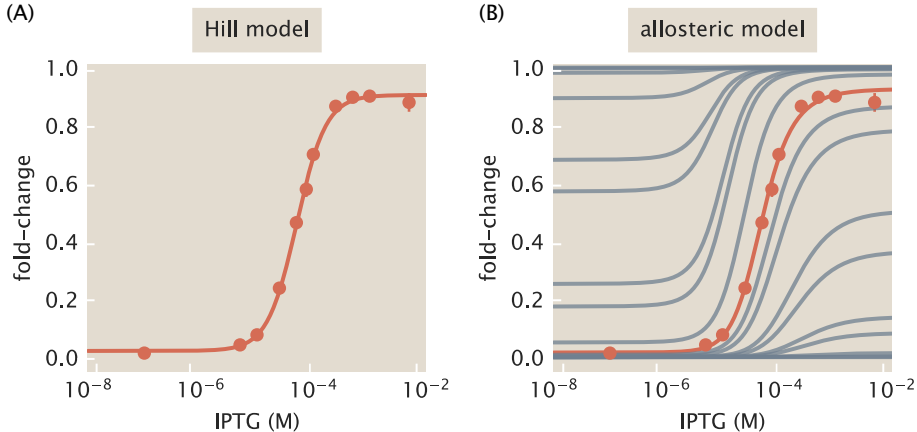


**Figure 19.** Predictive versatility of the Hill function versus allosteric models. (A) Measurements of the fold-change of a simple repression architecture as a function of IPTG concentration. Points and error bars represent the mean and standard error of ten biological replicates of repression of the O2 operator with 260 repressors per cell. (A) Solid line is the best-fit of the standard Hill function given in Equation 28. (B) Best-fit line for the data using the MWC model of allostery coupled with the thermodynamic model is in red. Gray lines represent predicted induction profiles of other combinations of repressor copy numbers and DNA binding energies. These predictions are made using only the parameters fit from a single strain. Tests of these predictions were shown in Figure 14(C).

parameter. Figure 19(A) shows Equation 28 applied to an induction profile of the *lac* simple repression motif with an O2 operator and 260 repressors per cell. Unsurprisingly, this equation can fit the data very nicely when all of the coefficients are properly determined. In fact, this fit is nearly indistinguishable from that obtained through a Monod-Wyman-Changeux (MWC) model inspired approach [66], as is shown in Figure 19(B). However, fitting a Hill function results in a single curve. In the Hill framework, for each induction profile we must fit Equation 28 once again for all parameters. As the parameters for an allosteric model have a direct connection to the biological properties of the repressor molecule, we can use the parameter values determined from one experimental circumstance to predict a wide swath of other induction profiles. Examples of such curves are shown as gray profiles in Figure 19(B).

What distinguishes allosteric models such as MWC and Koshland-Nemethy-Filmer (KNF, [102]) from Hill functions is that they make a tangible connection with what structural biology has taught us about the conformational states of proteins. The existence of inactive and active states implies that activity curves will be very special ratio of polynomials. While an individual fit may be comparable in quality to that obtained by a Hill function, the loss of this physical context results in a fit that has no predictive ability. The MWC and KNF models, however, open the door to a huge suite of predictions not only about experiments like those described in this review but also for biochemical experiments at the level of single molecules. For example, the allosteric treatment of induction hints at how mutating the repressor directly would change the behavior of the system. It's easy to hypothesize that mutations in the DNA binding domain would alter the binding energy of the repressor to the DNA  $\Delta\epsilon_R$  whereas mutations in the inducer domain would alter the  $K_A$  and  $K_I$  (Figure 13(A)). If we were to redo the analysis by fitting phenomenological Hill equations, we would be left in the dark as to how to predict the effect of either of these perturbations.

*Two-State vs Three-State Dynamics.* Most of the theoretical work on mRNA distribution dynamics has focused on the two-state model for a regulated promoter in which the promoter is treated as though it has two available states, inactive and active [71, 46, 49]. Indeed, the predictions from [67] shown in Figure 14(D) were calculated using this model. However, another critical question to be examined

in the context of theoretical models of transcriptional noise is the relative merits of the two-state and three-state models (for the three-state model see Figure 12). Note that within this framework, the unregulated promoter itself becomes an effective two-state model since we now acknowledge both the empty promoter and the promoter occupied by RNA polymerase. In this case, the mRNA distribution can be fitted with the parameters  $k_{on}^{(P)}$ ,  $k_{off}^{(P)}$ ,  $r$  and  $\gamma$  while still accounting for the variability in promoter copy number across the cell cycle and this is the strategy used in the parameter determination described in Figure 13(B).

We have found that it is possible to fit the full mRNA distribution using either the two-state or three-state models as already described in ref. [67]. However, to get a fully self-consistent parameter set in which the mean-fold change as described in both the thermodynamic and kinetic pictures are identical, it is necessary to resort to the three-state model that explicitly accounts for repressor and polymerase binding. Specifically, we demand that the repressor kinetic parameters  $k_{on}^{(R)}$  and  $k_{off}^{(R)}$  are consistent with the repressor copy number  $R$  and the repressor-DNA binding energy  $\Delta\varepsilon_R$ . The parameters reported in Figure 13(B) were determined using these constraints, giving identical results for the mean fold-change under both languages and not surprisingly, requiring the full three-state model for this self-consistent picture to emerge.

## 8. Simple Repression in Other Contexts

Thus far, we have focused on one realization of the simple repression architecture. But in fact, the way that cells use the simple regulatory architecture is much more diverse, as illustrated in Figure 20. Variants of this architecture provide alternative means for the cell to perform signal transduction. Like LacI, many repressors are inducible, whereby binding of a small-molecule signaling ligand reduces their ability to bind DNA. The identities of these ligands are generally related to the physiological role provided by the operon under control. For example, while LacI binds allolactose and is involved in lactose utilization, GalR binds galactose and this in turn provides control over galactose usage [20, 103]. Among those having a simple repression architecture, MprA has been reported to bind antimicrobial agents such as 4-dinitrophenol and carbonyl cyanide m-chlorophenylhydrazone (CCCP), and negatively regulate the expression of multidrug resistance pumps [104]. A related but opposite logic is also commonly observed, referred to as co-repression, where binding of a small-molecule ligand instead will enhance the binding of the repressor to DNA. For example, TrpR binds tryptophan and provides repression of the tryptophan biosynthesis pathway, as well as repressing its own expression [105].

In both induction and co-repression, signaling is achieved by a ligand internal to the cell. Another approach is to instead monitor the external environment directly, which is the role provided by two-component signal transduction systems [106]. Here, the signal detection is typically carried out by a transmembrane protein, a sensor histidine kinase, which then activates a transcription regulator by phosphorylation. Such sensors that activate repressors involved in simple repression architectures include PhoR, ArcB, and CpxA, which regulate the DNA binding activity of PhoB, ArcA, and CpxR, respectively. The repressor PhoB is involved in regulating phosphorus uptake and metabolism, while ArcA primarily acts as a repressor under anaerobic conditions [107, 108]. CpxR appears to act on at least 100 genes, in response to cell envelope stress, but also plays roles associated with motility, biofilm development, and multidrug resistance [109].

Cells have also devised ways to rapidly respond to stimuli by actively degrading regulatory proteins under specific stimuli. The DNA damage, or SOS, response provides one such example, which is mediated by the repressor LexA [110]. Under conditions of DNA damage, LexA undergoes a self-cleavage reaction that is further catalyzed by the protein RecA, and this provides de-repression of about 40 genes [111]. Toxin-antitoxin systems such as RelB-RelE serve as another example of this. While the toxin RelE is metabolically stable, with a cellular concentration dependent on the cell division time, the antitoxin RelB is actively degraded by the protease Lon and this can lead to a much shorter half-life [112, 113].

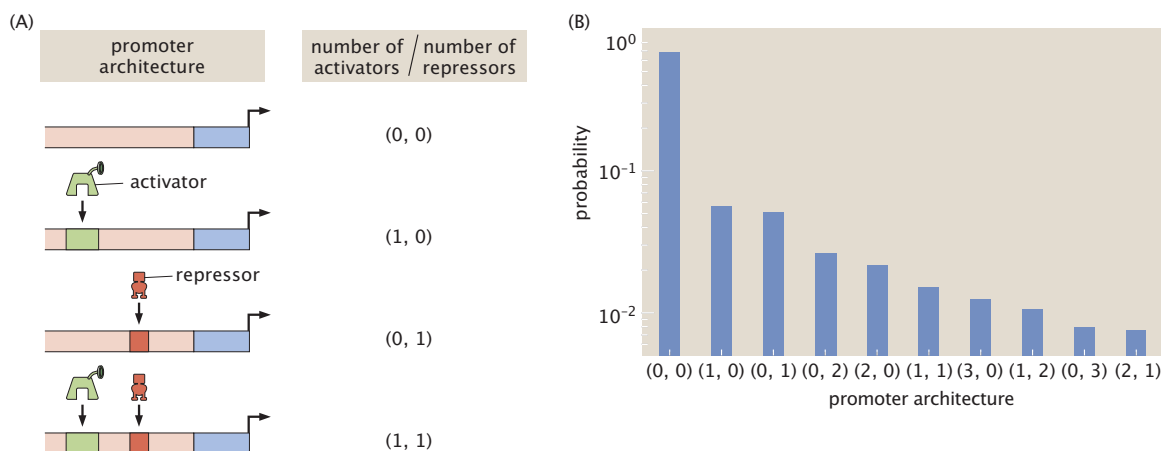


**Figure 20.** Simple repression in other contexts. Here we summarize several different modes of regulation that are observed at (0,1) architectures. Like LacI, many transcription factors are inducible and binding by a specific ligand leads to a loss of repression. Conversely, a number of transcription factors undergo co-repression and bind the DNA more strongly upon binding of a ligand to the repressor. For the examples identified, the transcription factor is shown in red text, while the ligand is shown in black. Several transcription factors appear as part of two component signal transduction systems, whose phosphorylation-dependent DNA-binding strength is changed by the activity of membrane bound sensor kinases. Lastly, repression can be modulated by changing the copy number of the repressor in response to stimuli. This can be achieved through self-cleavage (e.g., LexA), or by cellular proteases (e.g., RelB by Lon).

The examples provided here serve as a testbed for signal transduction strategies that demand further quantitative analysis and can be considered under the experimental-theoretical framework we have presented in this review. Table 1 gives us another way to get a sense of the diversity of simple repression motifs in *E. coli* by showing us the copy numbers of the key transcription factors involved in simple repression.

## 9. Beyond Simple Repression: Building New Pyramids

Of course, as we already showed in Figure 1, there is far more to transcriptional regulation than simple repression. Since the original development of the repressor-operator model by Jacob and Monod, the regulatory mechanisms of the *lac* operon have been resolved in exquisite detail, as shown diagrammatically on the left-hand side of Figure 7 [9]. The picture that has emerged is a rather complex one, in which Lac repressor monomers assemble into a dimer of dimers. These repressors can bind to two of the three operators found in the *lac* operon simultaneously, resulting in DNA looping and the stabilization of repressor action. Furthermore, the binding affinity of repressor to the DNA is modulated by inducer, which can be actively pumped into the cell by the Lac permease, which is one of the subjects of regulation by the repressor. This panoply of regulatory features calls for a complex theoretical description of the *lac* operon which can be nevertheless built on the parameters already obtained by building the simple repression pyramid.

One of the most interesting features of regulation in prokaryotes and eukaryotes alike comes in the form of DNA looping. Such biological action at a distance is seen in the wild-type *lac* operon itself, allowing us to dissect this ubiquitous regulatory mechanism quantitatively. Just as it was possible to engineer pared-down versions of the simple repression motif, similar exercises have been undertaken in the context of DNA looping, as shown in Figure 21(A). Looping has been explored in a wonderful series of experiments from the Müller-Hill lab [33, 69], and has also been elegantly treated using thermodynamic models [114]. These threads of research show how a pyramid of regulatory understanding for wild-type operons can be constructed, featuring multiple binding sites and DNA looping.

| protein | copy number in<br>glucose, minimal media | standard deviation<br>across 22 growth conditions | coefficient of variation |
|---------|--|---|--------------------------|
| HU      | 87425                                    | 28629   | 0.37                     |
| H-NS    | 22541                                    | 7181  | 0.24                     |
| IscR    | 7687                                     | 2603  | 0.49                     |
| Fur     | 6492                                     | 1707  | 0.29                     |
| Lrp     | 6092                                     | 1339  | 0.20                     |
| IHF     | 5018                                     | 1223  | 0.25                     |
| ArcA    | 3367                                     | 1030  | 0.24                     |
| CRP     | 2048                                     | 646   | 0.24                     |
| AlaS    | 1948                                     | 605   | 0.33                     |
| MprA    | 1085                                     | 516   | 0.61                     |
| PepA    | 1076                                     | 259   | 0.23                     |
| MetJ    | 990                                      | 231   | 0.31                     |
| CpxR    | 933                                      | 158   | 0.17                     |
| NsrR    | 872                                      | 189   | 1.78                     |
| PurR    | 826                                      | 165   | 0.24                     |
| FNR     | 609                                      | 236   | 0.49                     |
| LexA    | 560                                      | 177   | 0.32                     |
| CysB    | 523                                      | 124   | 0.33                     |
| AllR    | 206                                      | 68  | 0.43                     |
| FadR    | 186                                      | 75  | 0.34                     |
| RelB    | 178                                      | 61  | 0.53                     |
| TrpR    | 167                                      | 35  | 0.22                     |
| Cra     | 148                                      | 87  | 0.37                     |
| UidR    | 139                                      | 137   | 1.06                     |
| NagC    | 124                                      | 36  | 0.26                     |
| LacI    | 23                                       | 8   | 0.65                     |
| AcrR    | 21                                       | 10  | 1.08                     |
| DicA    | 20                                       | 6   | 0.40                     |
| BirA    | 19                                       | 7   | 0.50                     |
| AscG    | 17                                       | 12  | 0.62                     |
| NadR    | 16                                       | 4   | 0.26                     |
| PaaX    | 11                                       | 19  | 0.64                     |
| PhoB    | 7  | 5   | 0.45                     |

**Table 1.** Summary of transcription factors identified in (0,1) regulatory architectures. Protein copy numbers are per cell and were determined by mass spectrometry [29]. The values for HU and IHF were taken as the average of their individual subunits (HupA and HupB for HU, and IhfA and IhfB for IHF).



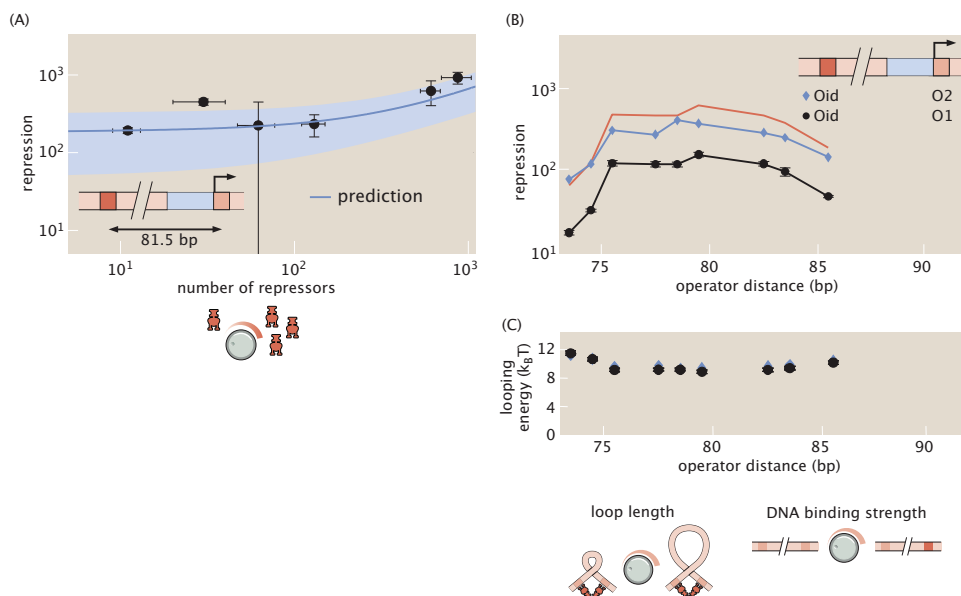


**Figure 21.** Regulatory action at a distance. The same minimal parameter set remains valid in the context of DNA looping, with the only requirement being to introduce a new parameter that captures the free energy of DNA looping. (A) Repression for the case of DNA looping as a function of the number of repressors per cell. (B,C) Operator swap experiment. In this case, for each DNA loop length, the operators that flank the loop were changed. (B) Using the Oid-O1 data to obtain the DNA looping free energy as a function of operator distance, the thermodynamic model makes a parameter-free prediction of how repression will work out in this case shown in the red curve. (C) Inferred looping free energy is the same regardless of which operators flank the loop. Adapted from [115].

Using the same minimal parameter set already identified in Figure 13(B), it is possible to make predictions about how the regulatory response will work in the context of DNA looping. For example, thermodynamic models of DNA looping identify one new key parameter with respect to those presented in Figure 13(B): the DNA looping free energy [114, 34]. By fitting this model to the repression corresponding to the looping architecture shown in Figure 21(A) for a particular number of repressors per cell, the model predicts the repression value as repressor copy number is systematically varied. Similarly, it is also possible to do an operator swap experiment in which the DNA loop itself, and hence the DNA looping free energy, is unchanged, but instead the binding sites that the repressor uses to form the loop are varied. Figure 21(B) shows the outcome of such experiments. In Figure 21(C), we also show that the inferred looping free energy is indifferent to the choice of operators used to induce the loop. The collection of results shown in Figure 21 provide further exciting evidence of the transferability of the minimal parameter set determined in the simple repression architecture.

In our opinion, one of the most surprising aspects about the state of the art in regulatory biology is our ignorance of regulation across genomes writ large. Even in the best understood of organisms, namely *E. coli*, we have no idea how more than half of the annotated genes are regulated, as we illustrated earlier in Figure 4 [30, 8, 116]. There we represented the circular *E. coli* genome with those operons for which there is some regulatory annotation shown in blue and those thus far featuring no such regulatory knowledge shown in red. Faced with the kind of ignorance revealed in that figure, there is no prospect of building up a regulatory dissection like that we have reviewed in the context of simple repression. To rectify this, we need to establish methods that will allow us, first of all, to simply draw the cartoons of how a given gene's regulatory apparatus is wired. Recent work has begun to develop tools that make it possible to go from regulatory sequence to the kind of regulatory architecture cartoons shown in Figure 1 [93, 96, 117]. Figure 22 exemplifies how a combination of mutagenesis, deep sequencing, mass

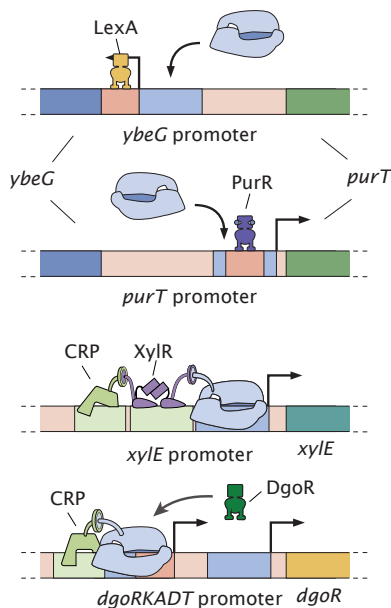


**Figure 22.** Beyond the *lac* operon in regulatory dissection. Using the Sort-Seq method it is now possible to identify regulatory architectures and the transcription factors that mediate them, making it possible to do regulatory dissections like that described here [96].

spectrometry and information theory has made it possible to take the uncharacterized genes reported in Figure 4 and figure out their regulatory architecture [93, 96]. Each time we identify how a given regulatory architecture is configured we are then poised to construct a new pyramid based upon minimal parameter sets like the one we describe here.

## 10. Gene regulation and statistical physics: Tactical Success But Strategic Failure?

An interesting reflection offered on the work presented here is that it should be viewed as a “tactical success but a strategic failure”. There are two aspects to this critique, and each is worth addressing. The first is that the architectures explored here are “synthetic” and thus anything we learn does not apply to the “real biology”. In response, we note that we set out more than a decade ago to understand gene regulation in bacteria in a quantitative and predictive manner with a view to exporting it to the entire regulatory genome not only of *E. coli*, but other more complex organisms as well. However, what we found was that even for the most well studied regulatory system, we had dispiritingly little quantitative understanding of how it would behave as the various “knobs” that control transcription were tuned. This demonstrated that we could not tackle the complexity of real endogenous promoters with potentially quite complex regulatory architectures without first proving to ourselves that we could understand the most basic unit already introduced in Jacob and Monod’s repressor-operator model and denoted here as the simple repression motif. Though we backpedaled from our original goals to do the most simple case, we think the work showcased here demonstrates that we have laid the groundwork for a full regulatory dissection of the *E. coli* genome. With the existence of methods like those highlighted in Figure 22 we are now poised to extend these kinds of regulatory dissections to the entire genome and believe that such work will unearth many generalizable principles [96].

The second thrust of the “tactical success but strategic failure” critique points out that, although we were able to find a single self-consistent minimal parameter set to describe regulation of the simple repression motif, it applies only to the particular conditions in which these specific strains were grown; if

the growth conditions are shifted then we will need to determine the relevant parameters all over again. This might be true, but to consider its weight we turn to an analogous example from the long history of the physics of materials. For a cubic material such as aluminum, we can measure the elastic constants ( $C_{11}$ ,  $C_{12}$  and  $C_{44}$ ) of single crystals. Now if we want to use those elastic constants to compute what will happen to a structure such as an airplane wing, we can confidently do so. However, if we alter the temperature of the metal away from that under which the constants were measured, the values of those elastic constants will change. Figuring out how elastic constants are modified by temperature entailed a great deal of subsequent work [118]. But acknowledging that a material response is subtle does not at all invalidate the original theory of linear elasticity, and for the gene regulatory situations considered here, we think it possible that a similar scenario might reveal itself. The first step is to make predictions and test them to determine whether different conditions do indeed require different parameters. The only way to actually *know* what happens in complex regulatory circuits is first to master a predictive understanding of the simplest case and subsequently build out from there.

Despite these worthy critiques, the point of this article was to show that with sufficient care, it is indeed possible to use a single minimal parameter set to describe a broad array of different regulatory situations. In our view, the results are sufficiently encouraging that it is now time to move to new systems such as systematic studies of the regulatory landscape of newly sequenced genomes of microbes from the ocean floor, for example. Having made the jump on the simple repression Rhodes, we are excited to see what comes of efforts of the kind described here in novel microorganisms and in the more challenging setting of multicellular organisms as well.

### Acknowledgments

We are grateful to a long list of generous colleagues who have helped us learn about this topic. We want to thank Stephanie Barnes, Lăcră Bîntu, James Boedicker, Rob Brewster, Robijn Bruinsma, Nick Buchler, Steve Busby, Jean-Pierre Changeux, Barak Cohen, Tal Einav, Uli Gerland, Ido Golding, Terry Hwa, Bill Ireland, Justin Kinney, Jane Kondev, Tom Kuhlman, Mitch Lewis, Sarah Marzen, Leonid Mirny, Alvaro Sanchez, Eran Segal, Marc Sherman, Kim Sneppen, Franz Weinert, Ned Wingreen and Jon Widom. We are grateful to Steve Busby, Ido Golding, Justin Kinney, Tom Kuhlman, Steve Quake and Alvaro Sanchez for reading the paper and providing important feedback. We are especially grateful to Nigel Orme who has worked with us for years to create illustrations that tell a conceptual and quantitative story about physical biology. It has also been a privilege to be entrusted by the National Science Foundation, the National Institutes of Health, The California Institute of Technology and La Fondation Pierre Gilles de Gennes with the funds that make this kind of research possible. Specifically we are grateful to the NIH for support through award numbers DP1 OD000217 (Director's Pioneer Award) and R01 GM085286. HGG was supported by the Burroughs Wellcome Fund Career Award at the Scientific Interface, the Sloan Research Foundation, the Human Frontiers Science Program, the Searle Scholars Program, the Shurl & Kay Curci Foundation, the Hellman Foundation, the NIH Director's New Innovator Award (DP2 OD024541-01), and an NSF CAREER Award (1652236).

## Figure 1 Theory Meets Figure 2 Experiments in the Study of Gene Expression Supplementary Information

Rob Phillips<sup>1,2,\*</sup>, Nathan M. Belliveau<sup>2</sup>, Griffin Chure<sup>2</sup>, Hernan G. Garcia<sup>3</sup>, Manuel Razo-Mejia<sup>2</sup>, Clarissa Scholes<sup>4</sup>

<sup>1</sup> Dept. of Physics, California Institute of Technology, Pasadena, California, U.S.A

<sup>2</sup> Division of Biology and Biological Engineering, California Institute of Technology, Pasadena, California, U.S.A

**3 Department of Molecular & Cell Biology, Department of Physics, Biophysics Graduate Group and Institute for Quantitative Biosciences-QB3, University of California, Berkeley, California, U.S.A**

**4 Department of Systems Biology, Harvard Medical School, Boston, Massachusetts, U.S.A**  
 \* **E-mail: phillips@pboc.caltech.edu**

This Appendix aims to spell out in full detail some of the key technical issues that arise in the attempt to make quantitative theoretical models of transcriptional regulation.

## 11. The occupancy hypothesis

The theoretical models presented in this work rely on the fundamental assumption that mRNA copy number can act as a proxy for the occupancy of the promoter by RNA polymerase. Only through this assumption are we able to relate experimentally accessible quantities, such as mRNA copy number or number of fluorescent proteins, to the promoter states that are considered theoretically. In this section we explore the validity and reach of this so-called occupancy hypothesis by considering the mathematical relationship between mRNA copy number,  $m$ , and the probability of finding RNA polymerase bound to the promoter,  $p_{bound}$ .

To make this analysis possible, we consider the simple model of transcription shown in Figure 23. As seen in the figure, we model each step between polymerase binding and mRNA production as a zero-order transition. In this context, the fraction of promoters in the process of initiating transcription,  $I$ , is given by

$$\frac{dI}{dt} = r_i p_{bound} - r_e I, \quad (29)$$

where  $r_i$  is the rate of initiation, and  $r_e$  is the rate of elongation. As elongation ensues, we will keep track of which base pair the polymerase is located on using the fraction of polymerase molecules occupying base pair  $j$ , which we denote by  $E_j$ . The fraction of molecules at the first base pair can be obtained by solving

$$\frac{dE_1}{dt} = r_e I - r_e E_1. \quad (30)$$

Similarly, for base pair  $j < N$ , where  $N$  is the length of the gene being transcribed, we have

$$\frac{dE_j}{dt} = r_e E_{j-1} - r_e E_j. \quad (31)$$

Finally, the fraction of polymerase molecules at the last base pair is given by

$$\frac{dE_N}{dt} = r_e E_{N-1} - r_t E_N, \quad (32)$$

where  $r_t$  is the rate of termination. Once an mRNA is terminated we assume that it is subject to degradation at a rate  $\gamma$  such that its concentration  $m$  is given by

$$\frac{dm}{dt} = r_t E_N - \gamma m. \quad (33)$$

By solving the system of equations shown above, we can then relate the magnitude predicted by our models,  $p_{bound}$ , to the measurable number of mRNA molecules  $m$ .

In order to solve for  $m$  using the above equations, we will assume steady-state such that all derivatives are zero. Further, due to the fact that every step in the process shown in Figure 23 is linear in the concentrations of the different molecular species, we can make use of a very convenient property of the system of equations. Specifically, we add up all equations together resulting in

$$0 = r_i p_{bound} - \gamma m \quad (34)$$

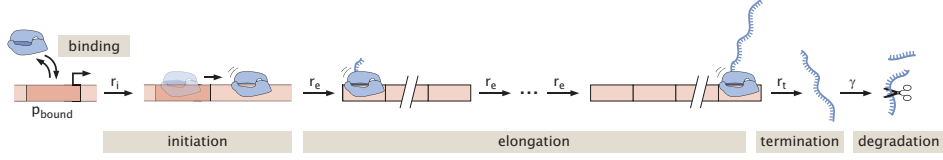


**Figure 23.** Simple model of mRNA production to probe the occupancy hypothesis. We assume that all steps from RNA polymerase binding to the termination and subsequent degradation of mRNA are described by zero-order kinetics.

such that

$$m = \frac{r_i}{\gamma} p_{bound}. \quad (35)$$

This provides us with the first important result. Specifically, under conditions of steady-state and assuming a transcriptional cascade composed of zero-order reactions, we find a simple linear relationship between the mRNA copy number and the occupancy state of the promoter, as determined through  $p_{bound}$ .

Under slightly different assumptions, the occupancy hypothesis can also be used to relate  $p_{bound}$  to the rate of mRNA production  $dm/dt$  as shown in Equation 1. First, we relax the assumption made above that all the processes described by Equations 29 through 33 are in steady-state. Instead we posit that only the processes up until Equation 33 reached this steady-state. To put this in other words, we will set only the derivatives in Equations 29 through 32 to zero. If we, once again, add up the system of equations, we arrive at

$$\frac{dm}{dt} = r_i p_{bound} - \gamma m. \quad (36)$$

Finally, we consider that mRNA degradation is negligible. This assumption true as long as the rate of initiation is faster than the degradation term such that  $r_i \ll \gamma m$ . Under this condition, we can neglect the last term on the right-hand side of Equation 36 leading to

$$\frac{dm}{dt} \approx r_i p_{bound} \quad (37)$$

which is Equation 1 if we identify the rate of transcriptional initiation  $r_i$  with the effective rate of mRNA production  $r$  used throughout the main text.

## 12. Equivalence of thermodynamic and statistical mechanical models of promoter occupancy

We next consider how the the statistical mechanical formulation of expression ( Bintu et al. [34]) compares with alternative thermodynamic formulations that use the language of dissociation constants (e.g. Buchler, Gerland, and Hwa [97, 37, 16], and introduced by Shea and Ackers [35, 36]). We begin with the statistical mechanical formulation of the simple repression architecture and calculate the probability of RNA polymerase bound to its target promoter,  $p_{bound}$ . We then consider how this formulation relates to thermodynamic formulations using dissociation constants. In doing so, we are able to show how these dissociation constants implicitly include a factor  $N_{NS}$  that was explicitly present in the statistical mechanical formulation and accounts for the reservoir of nonspecific binding sites on the genomic background.

Regardless of how we arrive at our model of transcriptional regulation, these models are all founded upon an assumption that the observed expression is proportional to the binding probability of RNA polymerase and that an assumption of steady-state is sufficiently valid. Here we begin by outlining the statistical mechanical formulation of the simple repression architecture [44]. We effectively treat the

genome as a reservoir containing  $N_{NS}$  nonspecific binding sites bound by RNA polymerase and a number of different transcription factors (Figure 10(A)). Due to the high concentration of DNA in the cell it is generally reasonable to assume that most, if not all of the transcription factors in the cell are bound to the genomic DNA [119, 91].

Here we would like to estimate the probability that RNA polymerase is bound to our simple repression promoter,  $p_{\text{bound}}$ , that is present on the genome. As shown in Figure 10(B), the promoter can either be empty, occupied by RNA polymerase, or occupied by a repressor (in this case, LacI). This probability depends on the difference in free energy associated with each particular state of the system. We will take as a reference state that where all RNA polymerase and LacI proteins are bound nonspecifically to the genomic background. Following this approach, the probability of bound RNA polymerase,  $p_{\text{bound}}$  can be found to be given by,

$$p_{\text{bound}} = \frac{\frac{P}{N_{NS}} e^{-\beta \Delta \varepsilon_P}}{1 + \frac{R}{N_{NS}} e^{-\beta \Delta \varepsilon_R} + \frac{P}{N_{NS}} e^{-\beta \Delta \varepsilon_P}}, \quad (38)$$

with  $\beta = \frac{1}{k_B T}$ , where  $k_B$  is the Boltzmann constant and  $T$  is the temperature of the system. Here,  $\Delta \varepsilon_P$  denotes the difference in binding energy when repressor binds the promoter, relative to nonspecific binding on the genome.  $\Delta \varepsilon_P$  similarly denotes the difference in binding energy when RNA polymerase binds the DNA.  $R$  and  $P$  represent the copy number per cell of repressor and RNA polymerase, respectively. Note that in our formulation, we have assumed that both the repressor and RNA polymerase are unable to bind simultaneously.

Now we can consider the thermodynamic approach that was taken by Buchler, Gerland, and Hwa [37]. In their work, the authors adopted and generalized the approach in the classic work of Shea and Ackers [35, 36] and so we shall begin there. In that classic work, Shea and Ackers developed a statistical mechanical model to describe the bacteriophage lambda switch, enumerating each possible configuration of the regulatory architecture. Following their approach, we will denote  $\Delta \dot{G}_P$  as the free energy for binding of RNA polymerase to the promoter, and  $\Delta \dot{G}_R$  for binding of LacI to the promoter. In their framework, the probability that RNA polymerase is bound to the promoter,  $p_{\text{bound}}$ , is then given by

$$p_{\text{bound}} = \frac{[P] e^{-\beta \Delta \dot{G}_P}}{1 + [P] e^{-\beta \Delta \dot{G}_P} + [R] e^{-\beta \Delta \dot{G}_R}}, \quad (39)$$

where  $[P]$  and  $[R]$  are the concentrations of unbound RNA polymerase and unbound LacI, respectively. The free energies can be related to corresponding dissociation constants through the standard relationship,

$$\Delta \dot{G}_P = k_B T \ln \frac{K_P}{c_0}, \quad (40)$$

and

$$\Delta \dot{G}_R = k_B T \ln \frac{K_R}{c_0}, \quad (41)$$

although note that in each case the argument of the logarithm is normalized by a standard state concentration  $c_0$ , normally taken to be 1 M. Here  $K_P$  is the dissociation constant for binding by RNA polymerase to the promoter, and  $K_R$  is the dissociation constant for binding of LacI to the promoter. These dissociation constants represent the concentration when each binding site is half-maximally occupied. Using these relationships between energy and dissociation constants in Equation 40 and Equation 41, we can re-write  $p_{\text{bound}}$  as,

$$p_{\text{bound}} = \frac{\frac{[P]}{K_P}}{1 + \frac{[P]}{K_P} + \frac{[R]}{K_R}}. \quad (42)$$

This is the thermodynamic representation that would be obtained following the approach of Buchler, Gerland, and Hwa [37]. Here we see that the probability is still determined by considering the set of

states available to the promoter, but with the corresponding Boltzmann weight for binding by RNA polymerase defined by  $[P]/K_P$ , and that of LacI by  $[R]/K_R$ .

Comparing the statistical mechanical equation of  $p_{\text{bound}}$  in Equation 38 with the thermodynamic representation in Equation 42 above, we find that

$$K_P = \frac{N_{NS}}{V_{\text{cell}}} e^{-\beta\Delta\varepsilon_P}, \quad (43)$$

and

$$K_R = \frac{N_{NS}}{V_{\text{cell}}} e^{-\beta\Delta\varepsilon_R}. \quad (44)$$

Here  $V_{\text{cell}}$  refers to the volume of the cell and is used to translate between protein copy numbers and concentrations. In the *in vivo* context considered here, the dissociation constants reflect binding by proteins that are otherwise assumed to be bound to the nonspecific genomic background, and will generally differ from what might be obtained from *in vitro* measurements [16]. Hence, we argue that both the statistical mechanical and thermodynamic formulations represent equivalent descriptions. The main distinction is that the statistical mechanical formulation is explicit in describing the nonspecific genomic background through the term  $N_{NS}$  and assuming one copy of the promoter.

### 13. The equilibrium assumption

Having established the conditions under which we can connect the probability of finding RNA polymerase bound to the promoter,  $p_{\text{bound}}$ , with the rate of mRNA production, we now ask whether it is reasonable to use the tools of statistical mechanics to calculate  $p_{\text{bound}}$ . While we are encouraged by the apparent validity of the theory based on the agreement with experimental data shown throughout the main text, here we will carefully consider the equilibrium assumption that underlies calculating  $p_{\text{bound}}$  in the context of our minimal parameter set (defined in Figure 13(B)). While it will be shown below that the rates of RNA polymerase binding and unbinding are incompatible with an equilibrium assumption for binding by RNA polymerase, we will find that under the weak-promoter approximation, there exists a regime where it is indeed reasonable to apply a statistical mechanical treatment to calculate  $p_{\text{bound}}$ .

First, we focus on the model of an unregulated promoter shown in Figure 24(A). Here, the promoter can be unoccupied or occupied by RNA polymerase. The fraction of promoters in each state is denoted by  $p_{\text{unbound}}$  and  $p_{\text{bound}}$ , respectively. When RNA polymerase is bound it can also initiate transcription at a rate  $r$ . Upon RNA polymerase escape from the promoter, the system is taken back to an unoccupied state. The rate of change in the fraction of occupied promoters is given by

$$\frac{dp_{\text{bound}}}{dt} = k_{\text{on}}^{(P)} p_{\text{unbound}} - k_{\text{off}}^{(P)} p_{\text{bound}} - r p_{\text{bound}} \quad (45)$$

while the rate of mRNA production can be written as

$$\frac{dm}{dt} = r p_{\text{bound}} \quad (46)$$

which corresponds to the rate of mRNA production as posited by the occupancy hypothesis.

We next seek to establish under what conditions we can calculate  $p_{\text{bound}}$  using statistical mechanics. In the equilibrium limit,  $p_{\text{bound}}$  for this unregulated promoter can be calculated using the states and weights defined in Figure 9(A) such that

$$p_{\text{bound}}^{\text{equil}} = \frac{\frac{P}{N_{NS}} e^{-\beta\Delta\varepsilon_p}}{1 + \frac{P}{N_{NS}} e^{-\beta\Delta\varepsilon_p}}. \quad (47)$$

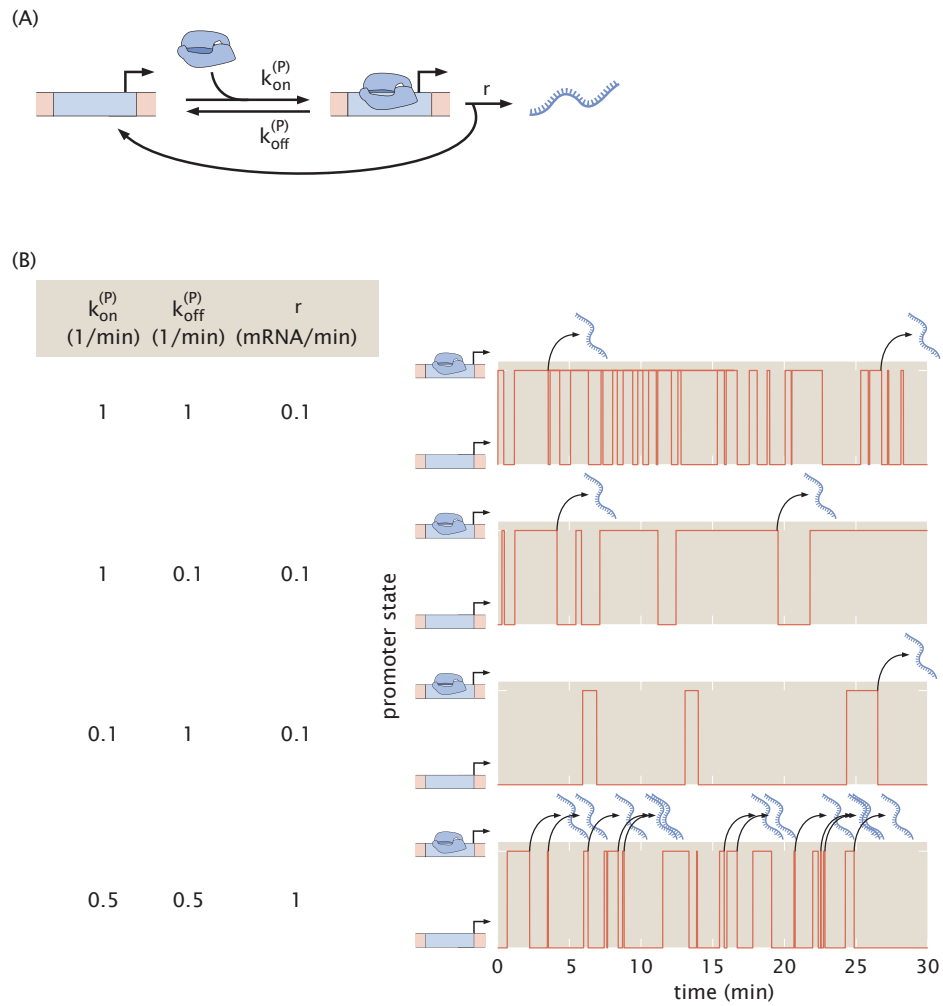


**Figure 24.** Exploring the equilibrium assumption for the constitutive promoter. (A) Kinetic scheme for a constitutive promoter. (B) Stochastic simulations of promoter state and initiation events for different parameters of the constitutive promoter.



In Appendix 12, we saw that this same expression can be written in the thermodynamic language as

$$p_{bound}^{equil} = \frac{\frac{[P]}{K_P}}{1 + \frac{[P]}{K_P}}, \quad (48)$$

where  $K_P$  is the dissociation constant between RNA polymerase and the promoter. This expression for  $p_{bound}^{equil}$  can be related to the scheme shown in Figure 24(A) by using  $[P]/K_P = k_{on}^{(P)}/k_{off}^{(P)}$  such that

$$p_{bound}^{equil} = \frac{k_{on}^{(P)}}{k_{on}^{(P)} + k_{off}^{(P)}}. \quad (49)$$

In order to calculate  $p_{bound}$  without enforcing equilibrium, we invoke steady-state in the fraction of occupied and unoccupied promoters such that Equation 45 can be written as

$$0 = k_{on}^{(P)} p_{unbound} - k_{off}^{(P)} p_{bound} - r p_{bound}. \quad (50)$$

We now make use of the fact that the probabilities are normalized,  $p_{bound} + p_{unbound} = 1$  in order to obtain

$$p_{bound} = \frac{k_{on}^{(P)}}{k_{on}^{(P)} + k_{off}^{(P)} + r}. \quad (51)$$

Clearly,  $p_{bound}$  in Equation 51 is not equal to  $p_{bound}^{equil}$  in Equation 49. The only way to recover  $p_{bound}^{equil}$  is for the rate of initiation  $r$  to be much slower than one of the other rates in the system. Namely, we need  $r \ll k_{on}^{(P)}$  or  $r \ll k_{off}^{(P)}$  such that  $k_{on}^{(P)} + k_{off}^{(P)} + r \approx k_{on}^{(P)} + k_{off}^{(P)}$ . These different limits are explored in Figure 24(B) through stochastic simulations that calculate the promoter state and initiation events as a function of time. In the first three simulations within Figure 24(B), we show how, when the conditions described above are met, the promoter cycles multiple times between its bound and unbound state before an initiation event ensues. This back-and-forth between the bound and unbound states leads to *quasiequilibrium*. That is, the fact that the transitions between the bound and unbound states are faster than the rate of initiation allows us to invoke separation of time scales such that, at each time point, we can use statistical mechanics to describe the equilibrium between these two states. However, if  $r$  is larger than these transition rates, most instances of the promoter being bound lead to an initiation event as shown in the last simulation in the Figure 24(B) and there is no longer a separation of time scales.

Interestingly, the inferred transition rates from Figure 13(B) do not fulfill this condition as  $k_{on}^{(P)}, k_{off}^{(P)} < r$ . Thus, at least *a priori*, equilibrium cannot be invoked to describe the transcription of an *unregulated lac* promoter. However, the successes of the theory at predicting experiments suggest that, under certain conditions, we are still allowed to invoke the quasi-equilibrium assumption for the *regulated lac* promoter.

We next consider the kinetic scheme for the regulated promoter, shown in Figure 25(A). The reader is reminded that this scheme does not make any assumption about the relative strength of each transition rate or about equilibrium. In this context, we are first interested in asking whether the probability of finding RNA polymerase bound to the promoter  $p(3) = p_{bound}$ , which we solved for in Equation 16, is equivalent to the same probability that can be calculated in the equilibrium case,  $p_{bound}^{equil}$ , shown in Equation 4.

To make progress, we rewrite  $p_{bound}^{equil}$  in Equation 4 in the language of dissociations constants

$$p_{bound}^{equil} = \frac{\frac{[P]}{K_P}}{1 + \frac{[P]}{K_P} + \frac{[R]}{K_R}}. \quad (52)$$

Invoking the identities introduced in Section 4.2 such that  $k_{on}^{(R)} = k_+^{(R)}[R]$  and  $k_{on}^{(P)} = k_+^{(P)}[P]$ , and the definition of the dissociations constant for repressor and RNA polymerase given by  $k_{off}^{(R)}/k_+^{(R)} = K_R$  and  $k_{off}^{(P)}/k_+^{(P)} = K_P$ , respectively, we obtain

$$p_{bound}^{equil} = \frac{\frac{k_{on}^{(P)}}{k_{off}^{(P)}}}{1 + \frac{k_{on}^{(P)}}{k_{off}^{(P)}} + \frac{k_{on}^{(R)}}{k_{off}^{(R)}}}. \quad (53)$$

In contrast,  $p_{bound}$  from Equation 16, which is absent of any assumption of equilibrium, is given by

$$p_{bound} = \frac{\frac{k_{on}^{(P)}}{k_{off}^{(P)}+r}}{1 + \frac{k_{on}^{(P)}}{k_{off}^{(P)}+r} + \frac{k_{on}^{(R)}}{k_{off}^{(R)}}}. \quad (54)$$

Again, as with the unregulated promoter, we find that the expression for  $p_{bound}$  is not equal to  $p_{bound}^{equil}$ . One way to alleviate this discrepancy is through the quasiequilibrium assumption noted above, requiring that the rate of RNA polymerase unbinding is much faster than the rate of initiation,  $k_{off}^{(P)} \ll r$ . However, Figure 13(B) reveals that  $k_{off}^{(P)} \approx r$  and not  $k_{off}^{(P)} \ll r$  as demanded above for the quasiequilibrium approximation to apply. Interestingly, at least for the case of simple repression considered here, we will see below that the equilibrium assumption can still be invoked under certain conditions for the calculation of the fold-change in gene expression.

In Equation 17 in the main text, we calculated the fold-change in gene expression corresponding to the kinetic scheme presented in Figure 12 and reproduced in Figure 25(A). This calculation made no assumption regarding equilibrium and resulted in

$$\text{fold-change} = \frac{1 + \frac{k_{on}^{(P)}}{k_{off}^{(P)}+r}}{1 + \frac{k_{on}^{(P)}}{k_{off}^{(P)}+r} + \frac{k_{on}^{(R)}}{k_{off}^{(R)}}}. \quad (55)$$

Our objective is then to determine under what limits we can reduce this fold-change to its equilibrium counterpart obtained in Equation 7 or in the context of the weak-promoter approximation shown in Equation 8.

As expected from our calculations on the applicability of equilibrium to derive  $p_{bound}$ , if we assume that  $k_{off}^{(P)} \ll r$ , Equation 55 reduces to the fold-change in equilibrium shown in Equation 7. We already saw that this limit is not consistent with the inferred rates. However, instead, consider the limit where  $k_{on}^{(P)} \ll k_{off}^{(P)} + r$ . In this case, we can neglect the term  $\frac{k_{on}^{(P)}}{k_{off}^{(P)}+r}$  in Equation 55 such that the fold-change reduces to

$$\text{fold-change} \approx \frac{1}{1 + \frac{k_{on}^{(R)}}{k_{off}^{(R)}}} = \frac{1}{1 + \frac{[R]}{K_R}}, \quad (56)$$

which corresponds to the fold-change in equilibrium under the weak-promoter approximation shown in Equations 8 and 9. In Figure 25(B) we explore this regime using stochastic simulations. The simulation reveals that, in this limit, the promoter mostly transitions between its repressor-occupied state and its empty state. Only rarely will the system transition to the RNA polymerase-bound state and, on these rare occasions, this event almost always leads to the initiation of transcription and the return of the promoter to its empty state. As a result, there is a clear separation of time scales between the process of repressor binding and unbinding and the subsequent steps in the transcriptional cascade. This separation

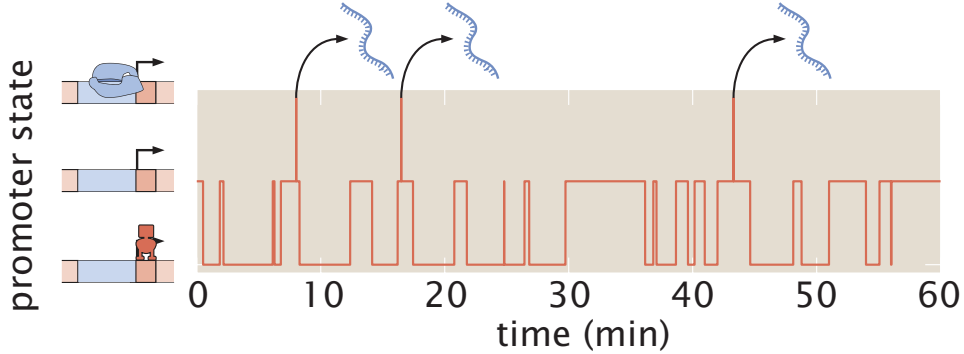


**Figure 25.** Exploring the equilibrium assumption for simple repression. Stochastic simulations of promoter state and initiation events for the kinetic scheme introduced in Figure 12 for different parameters of the regulated promoter, for the case where  $k_{on}^{(P)} \ll k_{off}^{(P)} + r$ . Here we observe many more binding and unbinding events by the repressor than by RNA polymerase, characteristic of our statistical mechanical description. The parameters used are  $k_{on}^{(P)} = 0.1 \text{ min}^{-1}$ ,  $k_{off}^{(P)} = 1 \text{ min}^{-1}$ ,  $k_{on}^{(R)} = 0.5 \text{ min}^{-1}$ ,  $k_{off}^{(R)} = 0.5 \text{ min}^{-1}$ , and  $r = 60 \text{ min}^{-1}$ .

of time scales justifies the applicability of the quasiequilibrium assumptions to calculate the fold-change in gene expression in terms of the probability of repressor binding.

As seen in Figure 13(B), our estimates for  $k_{on}^{(R)}$ ,  $k_{off}^{(R)}$  and  $r$  suggest that we are in this regime where the fold-change in gene expression can be calculated using the tools of statistical mechanics despite the fact that the probability of RNA polymerase binding to the promoter cannot be obtained using such equilibrium considerations. Thus, by considering fold-change instead of  $p_{bound}$  directly, we are able to ignore the potentially non-equilibrium behavior of RNA polymerase.

#### 14. The nonspecific genomic background

A simplifying assumption often made in thermodynamic models of transcription is the idea that the binding of transcription factors to nonspecific sites is characterized by a single binding energy as shown in Figure 26(A). In this case, the partition function for putting  $P$  polymerases on the nonspecific background is

$$Z_{NS}(P, N_{NS}) = \frac{N_{NS}^P}{P!} e^{-\beta P \varepsilon_{NS}}. \quad (57)$$

Of course, this is a convenient simplifying assumption that is pedagogically helpful, but raises the question of whether it masks some important effect. In fact, as we show in the remainder of this section, even when the nonspecific background is characterized by a distribution of energies, ultimately, it can be represented by an equation of the form Equation 57, but with the energy  $\varepsilon_{NS}$  replaced by an *effective energy*.

To get a feeling for how the effective energy arises, we begin with a toy model of the nonspecific background as shown in Figure 26(B). In this case, the  $P$  polymerases are distributed between the  $N_{NS}/2$  sites available with binding energy  $\varepsilon_1 = \bar{\varepsilon} + \Delta$  and the  $N_{NS}/2$  sites available with binding energy  $\varepsilon_2 = \bar{\varepsilon} - \Delta$  such that  $\bar{\varepsilon}$  is the mean non-specific binding energy. To compute the partition function, we need to sum over *all* the ways of distributing the  $P$  polymerases over the two nonspecific reservoirs. We imagine that the number bound on reservoir 1 is  $i$  and the number bound on reservoir 2 is  $P - i$ , and then sum over all  $i$  ranging from  $i = 0$  all the way to  $i = P$ , resulting in

$$Z_{NS} = \sum_{i=0}^P g_1(i) g_2(P-i) e^{-\beta [i\varepsilon_1 + (P-i)\varepsilon_2]}, \quad (58)$$

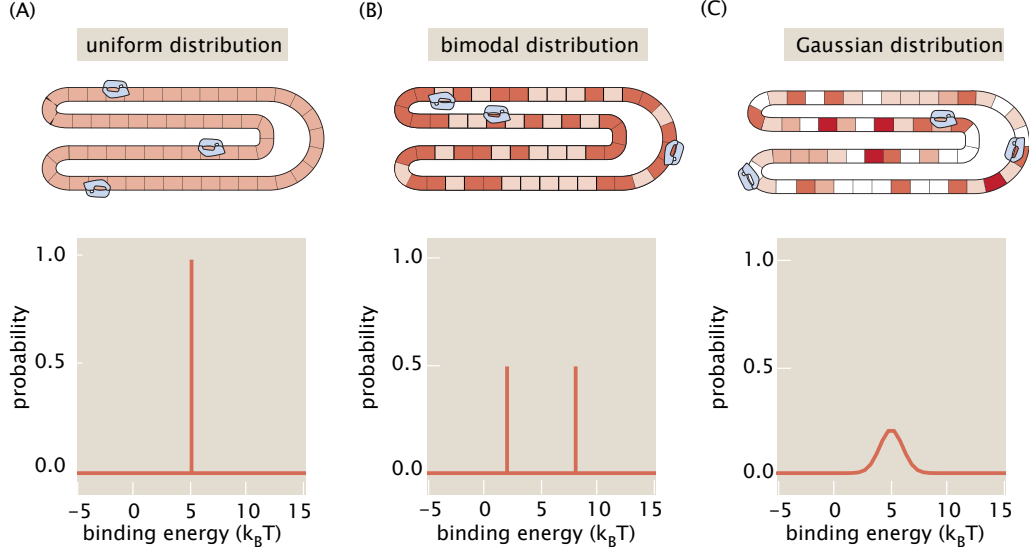


**Figure 26.** Increasingly sophisticated models of the nonspecific background. (A) Uniform background. (B) Two-state model of the nonspecific background. (C) Nonspecific binding energies characterized by a Gaussian distribution.

where  $g_1(i)$  is the number of ways of distributing  $i$  polymerases over the  $N_{NS}/2$  sites of reservoir 1 and  $g_2(P-i)$  is the number of ways of distributing  $P-i$  polymerases over the  $N_{NS}/2$  sites of reservoir 2. Because  $i \ll N_{NS}/2$ , we can write  $g_1(i)$  as

$$g_1(i) \approx \frac{\left(\frac{N_{NS}}{2}\right)^i}{i!} \quad (59)$$

and similarly write  $g_2(P-i)$  as

$$g_2(P-i) \approx \frac{\left(\frac{N_{NS}}{2}\right)^{P-i}}{(P-i)!}. \quad (60)$$

In light of these results, we can now rewrite the partition function for nonspecific binding as

$$Z_{NS} = \sum_{i=0}^P \frac{\left(\frac{N_{NS}}{2}\right)^P}{i!(P-i)!} e^{-\beta[i\varepsilon_1 + (P-i)\varepsilon_2]} \quad (61)$$

which can be rewritten as

$$Z_{NS} = \frac{\left(\frac{N_{NS}}{2}\right)^P}{P!} e^{-\beta P\varepsilon_2} \sum_{i=0}^P \frac{P!}{i!(P-i)!} e^{-\beta i(\varepsilon_1 - \varepsilon_2)}, \quad (62)$$

where we have multiplied the previous expression by  $P!/P! = 1$  in anticipation of beating our formula into the form of a binomial. Indeed, our sum is now of the form of a binomial allowing us to use

$$\sum_{i=0}^P \frac{P!}{i!(P-i)!} x^i = (1+x)^P. \quad (63)$$

As a result, we can write our partition function in the form

$$Z_{NS} = \frac{N_{NS}^P}{P!} \frac{1}{2^P} (e^{-\beta\varepsilon_2} (1 + e^{-\beta(\varepsilon_1 - \varepsilon_2)}))^P. \quad (64)$$

This should be compared with

$$Z_{NS} = \frac{N_{NS}^P}{P!} e^{-\beta P \varepsilon_{NS}} \quad (65)$$

which is the result for the partition function for the most simple model in which the nonspecific background is assumed to be uniform.

We now want to see whether our expression given in eqn. 64 is equivalent to the single reservoir model. By equating eqn. 64 and eqn. 65 and taking the log of both sides we have

$$\varepsilon_{NS} = k_B T \ln 2 + \varepsilon_2 - k_B T \ln (1 + e^{-\beta(\varepsilon_1 - \varepsilon_2)}) \quad (66)$$

We can simplify this by noting that the term involving the logarithm can be simplified as

$$\ln(1 + e^{-\beta(\varepsilon_1 - \varepsilon_2)}) = \ln(1 + e^{-2\beta\Delta}) \approx \ln(1 + 1 - 2\beta\Delta) \approx \ln 2 + \ln(1 - \beta\Delta), \quad (67)$$

where we have used the fact that  $\varepsilon_1 - \varepsilon_2 = 2\Delta$ . Given that  $\beta\Delta \ll 1$  (i.e. the energy difference between the two states is small), we can use the Taylor series  $\ln(1 - x) \approx -x$  with the result that

$$\varepsilon_{NS} = \bar{\varepsilon} \quad (68)$$

This result shows us that in the toy model of the nonspecific background of Figure 26(B), the two nonspecific backgrounds are equivalent to a single reservoir with an energy given by the mean of the energies of the two reservoirs, establishing that in this pedagogically motivated model we can use a single energy to describe the nonspecific background. Now let's move to the case of realistic distribution of nonspecific energies.

Figure 17 shows the distribution of nonspecific binding energies obtained by taking the energy matrix describing the binding of LacI and applying it to all sites across the *E. coli* genome (also see Figure 26(C) for a comparison with the other models considered thus far). Other examples of the distribution of nonspecific binding energies have been considered as well with similar outcome [97, 98]. As a result, we can write the number of binding sites with energy between  $E$  and  $E + dE$  as

$$n(E) = \frac{N_{NS}}{\sqrt{2\pi\sigma^2}} e^{-(E-\bar{\varepsilon})^2/2\sigma^2}, \quad (69)$$

where  $\bar{\varepsilon}$  is the mean of the distribution of nonspecific binding energies and  $\sigma$  provides a measure of the width of that distribution.

To compute the partition function for the binding of a polymerase, for example, to this nonuniform genomic background, we need to sum over all the microscopic states available to the polymerase. Symbolically, the quantity we need to evaluate is

$$Z_{NS} = \sum_E n(E) e^{-\beta E}. \quad (70)$$

In fact, since we are assuming a continuous distribution of energies, this really is an integral of the form

$$Z_{NS} = \int_{-\infty}^{\infty} e^{-\beta E} \frac{N_{NS}}{\sqrt{2\pi\sigma^2}} e^{-(E-\bar{\varepsilon})^2/2\sigma^2} dE. \quad (71)$$

This result can be rewritten as

$$Z_{NS} = \frac{N_{NS}}{\sqrt{2\pi\sigma^2}} e^{-\bar{\varepsilon}^2/2\sigma^2} \int_{-\infty}^{\infty} e^{-\frac{1}{2\sigma^2}[E^2 - 2E\bar{\varepsilon} + 2\sigma^2\beta E]} dE. \quad (72)$$

By completing the square, this integral results in

$$Z_{NS} = N_{NS} e^{-\beta\bar{\varepsilon}} e^{\beta^2\sigma^2/2} \quad (73)$$

which should be compared with the result we would get if we assumed a homogeneous nonspecific background with only a single binding energy  $\varepsilon_{NS}$  resulting in the form

$$Z_{NS} = N_{NS}e^{-\beta\varepsilon_{NS}} \quad (74)$$

By equating these two expressions, we find that we can treat the nonuniform background as though it were a homogenous genomic background with effective binding energy

$$\varepsilon_{eff} = \bar{\varepsilon} - \frac{\beta\sigma^2}{2}. \quad (75)$$

The result above considered a single polymerase or repressor molecule bound to the nonuniform nonspecific background. What happens in the case where we have  $P$  polymerases bound nonspecifically? Because each of those polymerases binds independently of the others (because the number of polymerases is of order  $10^3 - 10^4$  and the genome size is greater than  $10^6$  we don't need to worry about polymerases interfering with each other), the total partition function for all of these polymerases bound to the nonspecific background is given by

$$Z_{NS}(P, N_{NS}) = \frac{(\int_{-\infty}^{\infty} e^{-\beta E} \frac{N_{NS}}{\sqrt{2\pi\sigma^2}} e^{-(E-\bar{\varepsilon})^2/2\sigma^2} dE)^P}{P!} = \frac{N_{NS}^P e^{-\beta P \varepsilon_{eff}}}{P!}, \quad (76)$$

where once again  $\varepsilon_{eff} = \bar{\varepsilon} - \frac{\beta\sigma^2}{2}$  and this result shows that if the distribution of binding energies is Gaussian, then we can treat the nonspecific background as being equivalent to a uniform nonspecific background with energy  $\varepsilon_{eff}$ . The point of all of this analysis was simply to examine the validity of the convenient simplifying assumption of some thermodynamic models of treating the nonspecific background as uniform. As shown elsewhere [97, 98], this approximation is quite reasonable.

## 15. Accounting for the effect of nonspecific promoter occupancy

So far our statistical mechanical treatment of the simple repression architecture has treated the RNA polymerase and LacI proteins as isolated from the pool of other transcription factors that are also littered across the genomic DNA. In Figure 6 we plot the abundance of DNA-binding proteins per cell across a number of growth conditions using the proteomic study from Schmidt et al. [29]. These values include nucleoid-associated proteins that also bind the genomic DNA. For growth in M9 minimal media with 0.5% glucose, we find that there are about  $3 \times 10^5$  DNA-binding proteins per cell and we can use this to make a simple estimate of genomic occupancy by these proteins. Let us assume that each transcription factor binds the DNA as a dimer (this will vary with the transcription factor species) and occupies a DNA length of 15 bp (this varies from 7 bp to 38 bp in *E. coli* for transcription factors listed on RegulonDB; [8]). For growth in 0.5% glucose, we find that about 2.3 Mbp or about half the genome is occupied ( $15 \text{ bp} \times 3 \times 10^5 \text{ DNA-binding proteins} \times 1/2 \text{ dimers per protein}$ ).

Given the high occupancy of DNA-binding proteins on the genomic DNA estimated above, there might be some expectation that, in contrast to our current model of simple repression, the occupancy of the genome by these other DNA-binding proteins cannot be ignored. Here we consider the effect of their occupancy by adding an explicit set of states to represent the case where these additional DNA-binding proteins can occupy the roughly 60 bp promoter region of our simple repression architecture. For simplicity we assume that these proteins only bind nonspecifically, ignoring any potential sequence-specific effects. In Figure 27(A) we show the states and weights of the simple repression promoter, where we have included this additional set of states. We could have extended this further, either by treating each additional DNA-binding protein species separately, or by being more careful about our specification of these additional states. However, the point of this exercise is to see what effect the pool of nonspecifically

bound DNA-proteins might have on our model. We can calculate  $p_{\text{bound}}$  which, if we invoke the weak promoter approximation ( $\frac{P}{N_{NS}}e^{-\beta\Delta\varepsilon_P} \ll 1$ ), is given by

$$p_{\text{bound}} = \frac{\frac{P}{N_{NS}}e^{-\beta\Delta\varepsilon_P}}{1 + L \cdot \frac{C_{NS}}{N_{NS}} + \frac{R}{N_{NS}}e^{-\beta\Delta\varepsilon_R}}. \quad (77)$$

$L$  represents the number of ways other DNA-binding proteins may bind the promoter nonspecifically, and for simplicity is taken as the length of the promoter region ( $L \approx 60$  bp).  $C_{NS}$  represents the copy number of all other DNA-binding proteins bound to the genome that we noted earlier. Fold-change, which is the ratio of  $p_{\text{bound}}(R \geq 0)$  to  $p_{\text{bound}}(R = 0)$ , will then be given by

$$\text{fold-change} = \frac{1 + L \cdot \frac{C_{NS}}{N_{NS}}}{\frac{P}{N_{NS}}e^{-\beta\Delta\varepsilon_P}} \cdot \frac{\frac{P}{N_{NS}}e^{-\beta\Delta\varepsilon_P}}{1 + L \cdot \frac{C_{NS}}{N_{NS}} + \frac{R}{N_{NS}}e^{-\beta\Delta\varepsilon_R}}. \quad (78)$$

Here, the RNA polymerase components  $\frac{P}{N_{NS}}e^{-\beta\Delta\varepsilon_P}$  cancel out and upon some rearrangement, we find that

$$\text{fold-change} = \frac{1}{1 + \frac{R}{N_{NS}}e^{-\beta\Delta\varepsilon_R}(1 + L \cdot \frac{C_{NS}}{N_{NS}})^{-1}}. \quad (79)$$

Using  $C_{NS} \approx 1.5 \times 10^5$ , which is based on our estimate of the total DNA-binding protein copy number found above for growth in glucose (bound as dimers), we calculate a value of  $L \cdot \frac{C_{NS}}{N_{NS}} \approx 2$ . Importantly, we find that this additional term in our fold-change equation does not depend on the key parameters of our simple repression architecture, namely the repressor copy number or repressor binding energy, and we can arrive back to our original form of fold-change by a defining  $N'_{NS} = N_{NS} \times (1 + L \cdot \frac{C_{NS}}{N_{NS}})$ .

The estimates so far were based on assuming that cells grow in 0.5% glucose at a particular doubling rate. In different media, the growth rate will change leading also to a modulation in the total number of transcription factors: faster growing cells have a larger protein complement than their slower-growing counterparts. However, faster growing cells also have more copies of the genome as a means to keep up with the fast replication pace. Figure 27(B) shows that these two effects cancel each other out. Specifically, variations in the number of transcription factors as a result of changes in growth rate are counteracted by the corresponding change in the average genome copy number per cell such that the number of nonspecific binding proteins per base pair remains approximately constant throughout a wide range of growth conditions. As a result, the small effect of considering all nonspecifically bound transcription factors remains unaltered regardless of growth rate.

## References

Only a limited number of references from this vast field could be cited due to space considerations.

## References

1. F. Jacob, J. Monod, Genetic regulatory mechanisms in the synthesis of proteins, *J Mol Biol* 3 (1961) 318–56.
2. J. Monod, F. Jacob, General Conclusions - Teleonomic Mechanisms in Cellular Metabolism, Growth, and Differentiation, *Cold Spring Harbor Symposia on Quantitative Biology* 26 (1961) 389–401.
3. J. Monod, J.-P. Changeux, F. Jacob, Allosteric proteins and cellular control systems, *J Mol Biol* 6 (1963) 306–329.

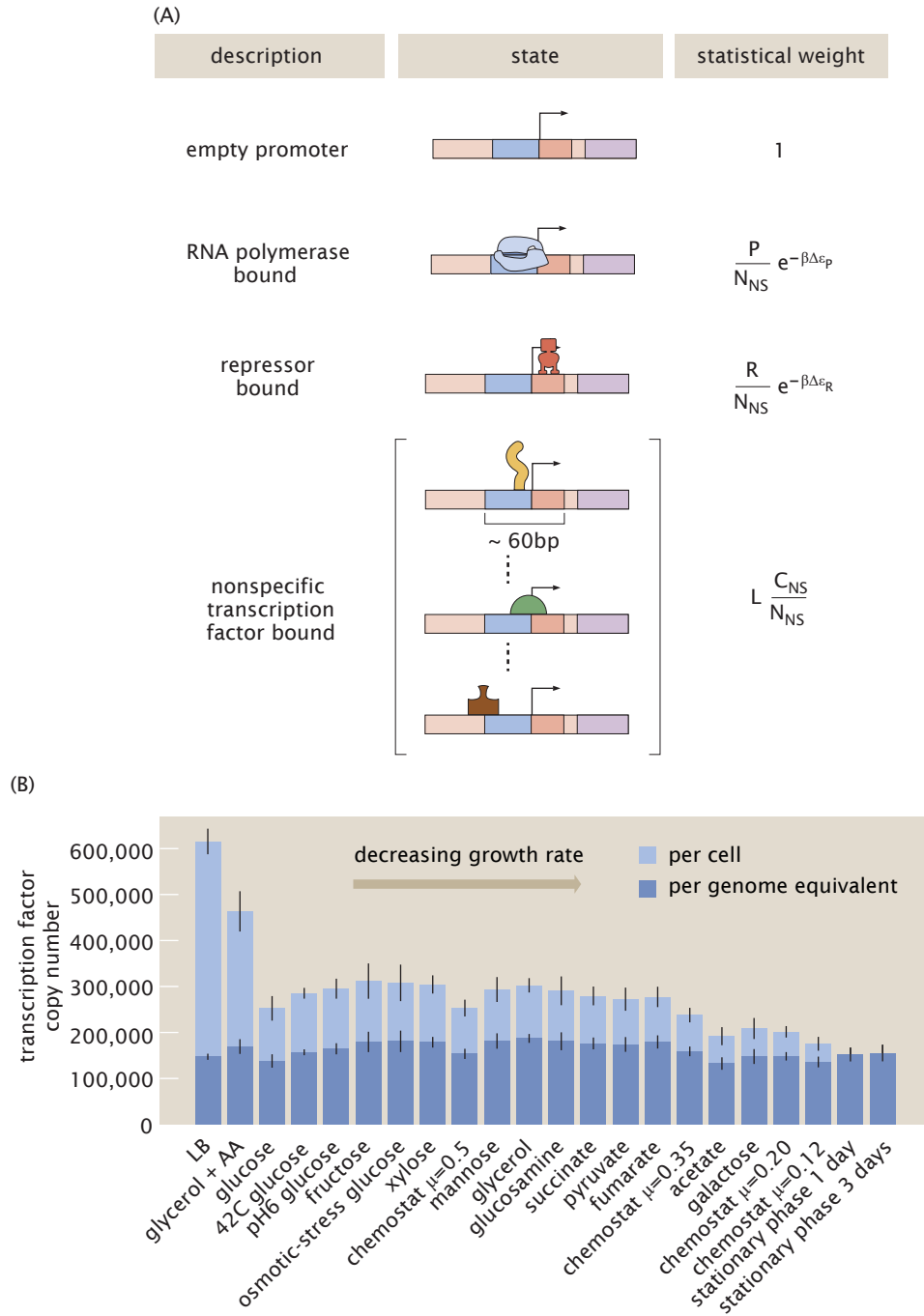


**Figure 27.** A crowded chromosome. (A) States and Weights for simple repression with a pool of nonspecific DNA binding proteins. RNA polymerase (light blue), a repressor, and other nonspecific DNA binding proteins compete for binding to a promoter. The  $R$  repressors and  $P$  RNA polymerase bind with energies  $\Delta\epsilon_R$  and  $\Delta\epsilon_P$ , respectively. In addition, there are  $C_{NS}$  DNA binding proteins per cell that can bind the promoter of length  $L \approx 60$  bp. These proteins bind nonspecifically and therefore only contribute an entropic term.  $N_{NS}$  represents the number of nonspecific binding sites on the genome. (B) Measured protein copy numbers are shown for DNA binding proteins in *E. coli* across 22 growth conditions. Protein copy numbers per cell were determined by Schmidt et al. [29] with proteins identified based on their annotation in EcoCyc. Error bars are propagated from the reported standard deviations. Protein copy numbers per genome equivalent were calculated by estimating the total genomic content as a function of growth rate using Cooper and Helmstetter's model of *E. coli* chromosomal replication [120, 121, 122].



4. R. J. Britten, E. H. Davidson, Gene regulation for higher cells: a theory, *Science* 165 (1969) 349–57.
5. G. Zubay, D. Schwartz, J. Beckwith, Mechanism of Activation of Catabolite-Sensitive Genes: A Positive Control System, *Proc Natl Acad Sci U S A* 66 (1970) 104–10.
6. M. Emmer, B. deCrombrughe, I. Pastan, R. Perlman, Cyclic AMP Receptor Protein of *E. coli*: Its Role in the Synthesis of Inducible Enzymes, *Proc Natl Acad Sci U S A* 66 (1970) 480–7.
7. M. Rydenfelt, H. G. Garcia, R. S. Cox III, R. Phillips, The Influence of Promoter Architectures and Regulatory Motifs on Gene Expression in *Escherichia coli*, *PLoS ONE* 9 (2014) e114347.
8. S. Gama-Castro, H. Salgado, A. Santos-Zavaleta, D. Ledezma-Tejeida, L. Muñoz-Rascado, J. S. García-Sotelo, K. Alquicira-Hernández, I. Martínez-Flores, L. Pannier, J. A. Castro-Mondragón, A. Medina-Rivera, H. Solano-Lira, C. Bonavides-Martínez, E. Pérez-Rueda, S. Alquicira-Hernández, L. Porrón-Sotelo, A. López-Fuentes, A. Hernández-Koutoucheva, V. D. Moral-Chávez, F. Rinaldi, J. Collado-Vides, RegulonDB version 9.0: high-level integration of gene regulation, coexpression, motif clustering and beyond, *Nucleic Acids Res* 44 (2016) D133–D143.
9. B. Müller-Hill, *The lac Operon: a short history of a genetic paradigm*, Walter de Gruyter, Berlin, New York, 1996.
10. B. Alberts, D. Bray, J. Lewis, M. Raff, K. Roberts, J. Watson, *Molecular Biology of the Cell*, 6th ed., W. W. Norton and Company, 2002.
11. U. Gerland, T. Hwa, On the selection and evolution of regulatory DNA motifs, *J Mol Evol* 55 (2002) 386–400.
12. J. Berg, S. Willmann, M. Lassig, Adaptive evolution of transcription factor binding sites, *BMC Evol Biol* 4 (2004) 42.
13. M. Lässig, From biophysics to evolutionary genetics: statistical aspects of gene regulation, *BMC Bioinform* 8 (2007) S7–21.
14. M. Lynch, K. Hagner, Evolutionary meandering of intermolecular interactions along the drift barrier, *Proc Natl Acad Sci U S A* 112 (2015) E30–8.
15. L. Saiz, J. M. Rubi, J. M. Vilar, Inferring the in vivo looping properties of DNA, *Proc Natl Acad Sci U S A* 102 (2005) 17642–5.
16. T. Kuhlman, Z. Zhang, M. H. S. Jr., T. Hwa, Combinatorial transcriptional control of the lactose operon of *escherichia coli*, *Proc Natl Acad Sci U S A* 104 (2007) 6043–8.
17. J. M. Vilar, L. Saiz, Reliable prediction of complex phenotypes from a modular design in free energy space: an extensive exploration of the lac operon, *ACS Synth Biol* 2 (2013) 576–86.
18. M. N. Alekshun, S. B. Levy, Regulation of chromosomally mediated multiple antibiotic resistance: the *mar* regulon., *J Mol Biol* 41 (1997) 2067–2075.
19. R. G. Martin, E. S. Bartlett, J. L. Rosner, M. E. Wall, Activation of the *Escherichia coli marA/soxS/rob* Regulon in Response to Transcriptional Activator Concentration, *J Mol Biol* 380 (2008) 278–284.
20. S. Semsey, M. Geanakopoulos, D. E. A. Lewis, S. Adhya, Operator-bound GalR dimers close DNA loops by direct interaction: tetramerization and inducer binding, *The EMBO journal* 21 (2002) 4349–4356.

21. S. Semsey, M. Y. Tolstorukov, K. Virnik, V. B. Zhurkin, S. Adhya, DNA trajectory in the Gal repressosome, *Genes Dev* 18 (2004) 1898–907.
22. L. Swint-Kruse, K. S. Matthews, Allostery in the LacI/GalR family: variations on a theme, *Curr Opin Microbiol* 12 (2009) 129–137.
23. I. B. Dodd, K. E. Shearwin, A. J. Perkins, T. Burr, A. Hochschild, J. B. Egan, Cooperativity in long-range gene regulation by the lambda CI repressor, *Genes Dev* 18 (2004) 344–54.
24. I. B. Dodd, K. E. Shearwin, J. B. Egan, Revisited gene regulation in bacteriophage lambda, *Curr Opin Genet Dev* 15 (2005) 145–52.
25. M. Ptashne, A genetic switch: phage lambda revisited, 3rd ed., Cold Spring Harbor Laboratory Press, Cold Spring Harbor, N.Y., 2004.
26. C. Zong, L. h. So, L. A. Sepulveda, S. O. Skinner, I. Golding, Lysogen stability is determined by the frequency of activity bursts from the fate-determining gene, *Mol Syst Biol* 6 (2010) 440.
27. R. Schleif, AraC protein, regulation of the l-arabinose operon in *Escherichia coli*, and the light switch mechanism of AraC action., *FEMS Microbiol Rev* 34 (2010) 779–796.
28. G.-W. Li, D. Burkhardt, C. Gross, J. S. Weissman, Quantifying Absolute Protein Synthesis Rates Reveals Principles Underlying Allocation of Cellular Resources, *Cell* 157 (2014) 624–635.
29. A. Schmidt, K. Kochanowski, S. Vedelaar, E. Ahrne, B. Volkmer, L. Callipo, K. Knoops, M. Bauer, R. Aebersold, M. Heinemann, The quantitative and condition-dependent *Escherichia coli* proteome, *Nature Biotech* 34 (2016) 104–111.
30. I. M. Keseler, J. Collado-Vides, A. Santos-Zavaleta, M. Peralta-Gil, S. Gama-Castro, L. Muniz-Rascado, C. Bonavides-Martinez, S. Paley, M. Krummenacker, T. Altman, P. Kaipa, A. Spaulding, J. Pacheco, M. Latendresse, C. Fulcher, M. Sarker, A. G. Shearer, A. Mackie, I. Paulsen, R. P. Gunsalus, P. D. Karp, EcoCyc: a comprehensive database of *Escherichia coli* biology, *Nucleic Acids Res* 39 (2010) D583–D590.
31. J. S. Rigden, *Hydrogen The Essential Element*, Harvard University Press, Cambridge, MA, 2003.
32. S. Oehler, E. R. Eismann, H. Krämer, B. M. Hill, The three operators of the *lac* operon cooperate in repression., *The EMBO journal* 9 (1990) 973–979.
33. S. Oehler, M. Amouyal, P. Kolkhof, B. von Wilcken Bergmann, B. M. Hill, Quality and position of the three *lac* operators of *E. coli* define efficiency of repression., *The EMBO journal* 13 (1994) 3348–3355.
34. L. Bintu, N. E. Buchler, H. G. Garcia, U. Gerland, T. Hwa, J. Kondev, R. Phillips, Transcriptional regulation by the numbers: models, *Curr Opin Genet Dev* 15 (2005) 116–24.
35. G. K. Ackers, A. D. Johnson, M. A. Shea, Quantitative model for gene regulation by lambda phage repressor, *Proc Natl Acad Sci U S A* 79 (1982) 1129–33.
36. M. A. Shea, G. K. Ackers, The OR control system of bacteriophage lambda. A physical-chemical model for gene regulation, *J Mol Biol* 181 (1985) 211–30.
37. N. E. Buchler, U. Gerland, T. Hwa, On schemes of combinatorial transcription logic, *Proc Natl Acad Sci U S A* 100 (2003) 5136–41.

38. J. M. Vilar, S. Leibler, DNA looping and physical constraints on transcription regulation, *J Mol Biol* 331 (2003) 981–9.
39. J. M. Vilar, C. C. Guet, S. Leibler, Modeling network dynamics: the lac operon, a case study, *J Cell Biol* 161 (2003) 471–6.
40. L. Bintu, N. E. Buchler, H. G. Garcia, U. Gerland, T. Hwa, J. Kondev, T. Kuhlman, R. Phillips, Transcriptional regulation by the numbers: applications, *Curr Opin Genet Dev* 15 (2005) 125–35.
41. J. Gertz, E. D. Siggia, B. A. Cohen, Analysis of combinatorial cis-regulation in synthetic and genomic promoters, *Nature* 457 (2009) 215–8.
42. M. S. Sherman, B. A. Cohen, Thermodynamic State Ensemble Models of cis-Regulation, *PLoS Comput Biol* 8 (2012) e1002407.
43. R. Phillips, Napoleon Is in Equilibrium, *Annu Rev Condens Matter Phys* 6 (2015) 85–111.
44. H. G. Garcia, R. Phillips, Quantitative dissection of the simple repression input-output function, *Proc Natl Acad Sci U S A* 108 (2011) 12173–8.
45. M. S. Ko, A stochastic model for gene induction, *J Theor Biol* 153 (1991) 181–94.
46. J. Peccoud, B. Ycart, Markovian Modeling of Gene-Product Synthesis 48 (1995) 222–234.
47. M. T. J. Record, W. Reznikoff, M. Craig, K. McQuade, P. Schlax, *Escherichia coli* RNA polymerase ( $\sigma^{70}$ ) promoters and the kinetics of the steps of transcription initiation, in: F. C. Neidhardt, R. C. III, J. L. Ingraham, E. C. C. Lin, K. B. Low, B. Magasanik, W. S. Reznikoff, M. Riley, M. Schaechter, H. E. Umbarger (Eds.), *In Escherichia coli and Salmonella Cellular and Molecular Biology*, ASM Press, Washington, DC, 1996, pp. 792–821.
48. T. B. Kepler, T. C. Elston, Stochasticity in transcriptional regulation: origins, consequences, and mathematical representations., *Biophys J.* 81 (2001) 3116–36.
49. A. Sanchez, J. Kondev, Transcriptional control of noise in gene expression, *Proc Natl Acad Sci U S A* 105 (2008) 5081–6.
50. V. Shahrezaei, P. S. Swain, Analytical distributions for stochastic gene expression, *Proc Natl Acad Sci U S A* 105 (2008) 17256–61.
51. H. G. Garcia, A. Sanchez, T. Kuhlman, J. Kondev, R. Phillips, Transcription by the numbers redux: experiments and calculations that surprise, *Trends Cell Biol* 20 (2010) 723–733.
52. D. Michel, How transcription factors can adjust the gene expression floodgates, *Prog Biophys Mol Biol* 102 (2010) 16–37.
53. R. Schleif, J. T. Lis, The regulatory region of the l-arabinose operon: A physical, genetic and physiological study, *J Mol Biol* 95 (1975) 417–431.
54. S. Ogden, D. Haggerty, C. M. Stoner, D. Kolodrubetz, R. Schleif, The *Escherichia coli* L-arabinose operon: binding sites of the regulatory proteins and a mechanism of positive and negative regulation., *Proc Natl Acad Sci U S A* 77 (1980) 3346–50.
55. T. M. Dunn, S. Hahn, S. Ogden, R. F. Schleif, An operator at -280 base pairs that is required for repression of *araBAD* operon promoter: addition of DNA helical turns between the operator and promoter cyclically hinders repression, *Proc Natl Acad Sci U S A* 81 (1984) 5017–20.

56. L. Saiz, J. M. Vilar, Ab initio thermodynamic modeling of distal multisite transcription regulation, *Nucleic Acids Res* 36 (2008) 726–31.
57. Y. Setty, A. E. Mayo, M. G. Surette, U. Alon, Detailed map of a cis-regulatory input function, *Proc Natl Acad Sci U S A* 100 (2003) 7702–7.
58. I. Golding, J. Paulsson, S. M. Zawilski, E. C. Cox, Real-time kinetics of gene activity in individual bacteria, *Cell* 123 (2005) 1025–36.
59. N. Rosenfeld, J. W. Young, U. Alon, P. S. Swain, M. B. Elowitz, Gene regulation at the single-cell level, *Science* 307 (2005) 1962–5.
60. A. Bakk, R. Metzler, K. Sneppen, Sensitivity of OR in phage lambda, *Biophys J* 86 (2004) 58–66.
61. L. Zeng, S. O. Skinner, C. Zong, J. Sippy, M. Feiss, I. Golding, Decision making at a subcellular level determines the outcome of bacteriophage infection, *Cell* 141 (2010) 682–91.
62. L. Cui, I. Murchland, K. E. Shearwin, I. B. Dodd, Enhancer-like long-range transcriptional activation by lambda ci-mediated dna looping, *Proc Natl Acad Sci U S A* 110 (2013) 2922–7.
63. L. A. Sepulveda, H. Xu, J. Zhang, M. Wang, I. Golding, Measurement of gene regulation in individual cells reveals rapid switching between promoter states, *Science* 351 (2016) 1218–22.
64. J. Gunawardena, Models in biology: ‘accurate descriptions of our pathetic thinking’, *BMC Bio* 12 (2014) 29.
65. D. R. H. Jones, M. F. Ashby, *Engineering Materials 1: An Introduction to Properties, Applications and Design* 4th Edition, Butterworth-Heinemann, Waltham, MA, 2012.
66. M. Razo-Mejia, S. L. Barnes, N. M. Belliveau, G. Chure, T. Einav, M. Lewis, R. Phillips, Tuning Transcriptional Regulation through Signaling: A Predictive Theory of Allosteric Induction, *Cell Syst* 6 (2018) 456–469 e10.
67. D. L. Jones, R. C. Brewster, R. Phillips, Promoter architecture dictates cell-to-cell variability in gene expression, *Science* 346 (2014) 1533–6.
68. M. Razo-Mejia, R. Phillips, First-principles prediction of the information processing capacity of a simple genetic circuit, Manuscript in preparation. (2018).
69. J. Muller, S. Oehler, B. Muller-Hill, Repression of *lac* promoter as a function of distance, phase and quality of an auxiliary *lac* operator, *J Mol Biol* 257 (1996) 21–9.
70. R. C. Brewster, F. M. Weinert, H. G. Garcia, D. Song, M. Rydenfelt, R. Phillips, The transcription factor titration effect dictates level of gene expression, *Cell* 156 (2014) 1312–23.
71. L. H. So, A. Ghosh, C. Zong, L. A. Sepulveda, R. Segev, I. Golding, General properties of transcriptional time series in *Escherichia coli*, *Nat Genet* 43 (2011) 554–60.
72. F. M. Weinert, R. C. Brewster, M. Rydenfelt, R. Phillips, W. K. Kegel, Scaling of gene expression with transcription-factor fugacity, *Phys Rev Lett* 113 (2014) 258101.
73. T. Dobzhansky, Nothing in Biology Makes Sense except in the Light of Evolution, *The American Biology Teacher* 35 (1973) 125–129.
74. M. Razo-Mejia, J. Boedicker, D. Jones, A. DeLuna, J. Kinney, R. Phillips, Comparison of the theoretical and real-world evolutionary potential of a genetic circuit, *Phys Biol* 11 (2014) 026005.

75. F. J. Poelwijk, M. G. J. de Vos, S. J. Tans, Tradeoffs and Optimality in the Evolution of Gene Regulation, *Cell* 146 (2011) 462–470.
76. F. J. Poelwijk, P. D. Heyning, M. G. de Vos, D. J. Kiviet, S. J. Tans, Optimality and evolution of transcriptionally regulated gene expression, *BMC Systems Biology* 5 (2011) 128.
77. A. Dawid, D. J. Kiviet, M. Kogenaru, M. de Vos, S. J. Tans, Multiple peaks and reciprocal sign epistasis in an empirically determined genotype-phenotype landscape, *Chaos* 20 (2010) 026105.
78. E. Dekel, U. Alon, Optimality and evolutionary tuning of the expression level of a protein, *Nature* 436 (2005) 588–92.
79. M. Tuğrul, T. Paixão, N. H. Barton, G. Tkačik, Dynamics of Transcription Factor Binding Site Evolution, *PLoS Genet* 11 (2015) e1005639.
80. R. Daber, M. A. Sochor, M. Lewis, Thermodynamic analysis of mutant lac repressors, *J Mol Biol* 409 (2011) 76–87.
81. J. Elf, G. W. Li, X. S. Xie, Probing transcription factor dynamics at the single-molecule level in a living cell, *Science* 316 (2007) 1191–4.
82. P. Hammar, M. Wallden, D. Fange, F. Persson, O. Baltekin, G. Ullman, P. Leroy, J. Elf, Direct measurement of transcription factor dissociation excludes a simple operator occupancy model for gene regulation, *Nat Genet* 46 (2014) 405–8.
83. H. Xu, L. A. Sepulveda, L. Figard, A. M. Sokac, I. Golding, Combining protein and mrna quantification to decipher transcriptional regulation, *Nat Methods* 12 (2015) 739–42.
84. W. K. Cho, N. Jayanth, B. P. English, T. Inoue, J. O. Andrews, W. Conway, J. B. Grimm, J. H. Spille, L. D. Lavis, T. Lionnet, I. Cisse, Rna polymerase ii cluster dynamics predict mrna output in living cells, *eLife* 5 (2016).
85. H. G. Garcia, A. Sanchez, J. Q. Boedicker, M. Osborne, J. Gelles, J. Kondev, R. Phillips, Operator sequence alters gene expression independently of transcription factor occupancy in bacteria, *Cell Rep* 2 (2012) 150–61.
86. T. H. Leung, A. Hoffmann, D. Baltimore, One nucleotide in a kappaB site can determine cofactor specificity for NF-kappaB dimers, *Cell* 118 (2004) 453–64.
87. S. H. Meijsing, M. A. Pufall, A. Y. So, D. L. Bates, L. Chen, K. R. Yamamoto, DNA binding site sequence directs glucocorticoid receptor structure and activity, *Science* 324 (2009) 407–10.
88. J. Estrada, F. Wong, A. DePace, J. Gunawardena, Information integration and energy expenditure in gene regulation, *Cell* 166 (2016) 234–44.
89. C. Li, F. Cesbron, M. Oehler, M. Brunner, T. Höfer, Frequency Modulation of Transcriptional Bursting Enables Sensitive and Rapid Gene Regulation, *Cell Sys* (2018) 1–27.
90. W. Runzi, H. Matzura, *In vivo* distribution of ribonucleic acid polymerase between cytoplasm and nucleoid in escherichia coli, *J Bacteriol* 125 (1976) 1237–9.
91. Y. Kao-Huang, A. Revzin, A. P. Butler, P. O’Conner, D. W. Noble, P. H. von Hippel, Nonspecific dna binding of genome-regulating proteins as a biological control mechanism: measurement of dna-bound *Escherichia coli* lac repressor *in vivo*, *Proc Natl Acad Sci U S A* 74 (1977) 4228–32.

92. F. Garza de Leon, L. Sellars, M. Stracy, S. J. W. Busby, A. N. Kapanidis, Tracking Low-Copy Transcription Factors in Living Bacteria: The Case of the lac Repressor, *Biophys J* 112 (2017) 1316–1327.
93. J. B. Kinney, A. Murugan, C. G. Callan, E. C. Cox, Using deep sequencing to characterize the biophysical mechanism of a transcriptional regulatory sequence., *Proceedings of the National Academy of Sciences* 107 (2010) 9158–9163.
94. R. C. Brewster, D. L. Jones, R. Phillips, Tuning promoter strength through RNA polymerase binding site design in *Escherichia coli*, *PLoS Comput Biol* 8 (2012) e1002811.
95. T. E. Kuhlman, E. C. Cox, Dna-binding-protein inhomogeneity in *e. coli* modeled as biphasic facilitated diffusion, *Phys Rev E Stat Nonlin Soft Matter Phys* 88 (2013) 022701.
96. N. M. Belliveau, S. L. Barnes, W. T. Ireland, D. L. Jones, M. J. Sweredoski, A. Moradian, S. Hess, J. B. Kinney, R. Phillips, Systematic approach for dissecting the molecular mechanisms of transcriptional regulation in bacteria, *Proc Natl Acad Sci U S A* 115 (2018) E4796–805.
97. U. Gerland, J. D. Moroz, T. Hwa, Physical constraints and functional characteristics of transcription factor-DNA interaction, *Proc Natl Acad Sci U S A* 99 (2002) 12015–20.
98. A. M. Sengupta, M. Djordjevic, B. I. Shraiman, Specificity and robustness in transcription control networks, *Proc Natl Acad Sci U S A* 99 (2002) 2072–7.
99. S. L. Barnes, N. M. Belliveau, W. T. Ireland, J. B. Kinney, R. Phillips, Mapping DNA sequence to transcription factor binding energy in vivo, *bioRxiv* (2018) 331124.
100. J. K. Rogers, C. D. Guzman, N. D. Taylor, S. Raman, K. Anderson, G. M. Church, Synthetic biosensors for precise gene control and real-time monitoring of metabolites, *Nucleic Acids Res* 43 (2015) 7648–7659.
101. J. Rohlhill, N. R. Sandoval, E. T. Papoutsakis, Sort-Seq approach to engineering a formaldehyde-inducible promoter for dynamically regulated *Escherichia coli* growth on methanol, *ACS Synth Biol* 6 (2017) 1584–1595.
102. J. Koshland, D. E., G. Nemethy, D. Filmer, Comparison of experimental binding data and theoretical models in proteins containing subunits, *Biochemistry* 5 (1966) 365–85.
103. S. Oehler, S. Alberti, B. Müller-Hill, Induction of the lac promoter in the absence of DNA loops and the stoichiometry of induction, *Nucleic Acids Res* 34 (2006) 606–612.
104. A. Brooun, J. J. Tomashek, K. Lewis, Purification and ligand binding of EmrR, a regulator of a multidrug transporter, *J Bacteriol* 181 (1999) 5131–5133.
105. J. Yang, A. Gunasekera, T. A. Lavoie, L. Jin, D. E. A. Lewis, J. Carey, *In vivo* and *in vitro* Studies of TrpR-DNA Interactions, *J Mol Biol* 258 (1996) 37–52.
106. M. T. Laub, M. Goulian, Specificity in Two-Component Signal Transduction Pathways, *Annu Rev Genet* 41 (2007) 121–145.
107. B. L. Wanner, Gene regulation by phosphate in enteric bacteria, *J Cell Biochem* 51 (1993) 47–54.
108. R. Malpica, G. R. P. Sandoval, C. Rodríguez, B. Franco, D. Georgellis, Signaling by the *arc* two-component system provides a link between the redox state of the quinone pool and gene expression, *Antioxid Redox Signal* 8 (2006) 781–795.

109. N. Ruiz, T. J. Silhavy, Sensing external stress: watchdogs of the *Escherichia coli* cell envelope, *Curr Opin Microbiol* 8 (2005) 122–126.
110. J. W. Little, D. W. Mount, The SOS regulatory system of *Escherichia coli*, *Cell* 29 (1982) 11–22.
111. K. C. Giese, C. B. Michalowski, J. W. Little, RecA-Dependent Cleavage of LexA Dimers, *J Mol Biol* 377 (2008) 148–161.
112. I. Cataudella, K. Sneppen, K. Gerdes, N. Mitarai, Conditional Cooperativity of Toxin - Antitoxin Regulation Can Mediate Bistability between Growth and Dormancy, *PLoS Comp Bio* 9 (2013) e1003174.
113. M. Overgaard, J. Borch, K. Gerdes, RelB and RelE of *Escherichia coli* form a tight complex that represses transcription via the ribbon-helix-helix motif in RelB., *J Mol Biol* 394 (2009) 183–196.
114. J. M. Vilar, L. Saiz, DNA looping in gene regulation: from the assembly of macromolecular complexes to the control of transcriptional noise, *Curr Opin Genet Dev* 15 (2005) 136–44.
115. J. Q. Boedicker, H. G. Garcia, R. Phillips, Theoretical and experimental dissection of DNA loop-mediated repression, *Phys Rev Lett* 110 (2013) 018101.
116. X. Fang, A. Sastry, N. Mih, D. Kim, J. Tan, J. T. Yurkovich, C. J. Lloyd, Y. Gao, L. Yang, B. Ø. Palsson, Global transcriptional regulatory network for *Escherichia coli* robustly connects gene expression to transcription factor activities, *Proc Natl Acad Sci U S A* 114 (2017) 10286–91.
117. S. Kosuri, D. B. Goodman, G. Cambray, V. K. Mutalik, Y. Gao, A. P. Arkin, D. Endy, G. M. Church, Composability of regulatory sequences controlling transcription and translation in *Escherichia coli*., *Proc Natl Acad Sci U S A* 110 (2013) 14024–9.
118. R. Phillips, *Crystals, Defects and Microstructures*, Cambridge University Press, New York, 2001.
119. P. L. deHaseth, C. A. Gross, R. R. Burgess, M. T. J. Record, Measurement of binding constants for protein-DNA interactions by DNA-cellulose chromatography, *Biochemistry* 16 (1977) 4777–83.
120. S. Cooper, C. E. Helmstetter, Chromosome replication and the division cycle of *Escherichia coli* Br, *J Mol Biol* 31 (1968) 519–540.
121. P. P. Dennis, H. Bremer, Modulation of Chemical Composition and Other Parameters of the Cell at Different Exponential Growth Rates, *EcoSal Plus* 3 (2008).
122. T. E. Kuhlman, E. C. Cox, Gene location and DNA density determine transcription factor distributions in *Escherichia coli*, *Mol Syst Biol* 8 (2012) 610.